ISTANBUL TECHNICAL UNIVERSITY ★ GRADUATE SCHOOL

POLYAMIDE SYNTHESIS FOR REVERSE OSMOSIS MEMBRANE AND SUBSTRATE OPTIMIZATION

M. Sc. THESIS

Büşra ARSLAN

Department of Nanoscience and Nanoengineering

Nanoscience and Nanoengineering Programme

February 2024

ISTANBUL TECHNICAL UNIVERSITY ★ GRADUATE SCHOOL

POLYAMIDE SYNTHSIS FILM FOR REVERSE OSMOSIS MEMBRANE AND SUBSTRATE OPTIMIZATION

M. Sc. THESIS

Büşra ARSLAN
(513201027)

Department of Nanoscience and Nanoengineering

Nanoscience and Nanoengineering Programme

Thesis Advisor: Prof. Dr. Levent TRABZON
Thesis Co-Advisor: Asst Prof. Dr. Çiğdem TAŞDELEN YÜCEDAĞ

February 2024

ISTANBUL TEKNİK ÜNİVERSİTESİ ★ LİSANSÜSTÜ EĞİTİM ENSTİTÜSÜ

REVERSE OSMOSİZ MEMBRANLAR İÇİN POLYAMİD İNCE FİLM SENTEZİ VE DESTEK YÜZEY OPTİMİZASYONU

YÜKSEK LİSANS TEZİ

Büşra ARSLAN
(513201027)

Nanobilim ve Nanomühendislik Anabilim Dalı

Nanobilim ve Nanomühendislik

Tez Danışmanı: Prof Dr. Levent TRABZON
Eş Danışman: Dr. Öğr. Çiğdem TAŞDELEN YÜCEDAĞ

Şubat 2024

Büşra ARSLAN, a M.Sc. student of ITU Graduate School student ID 513201027, successfully defended the thesis/dissertation entitled “POLYAMIDE SYNTHESIS FOR REVERSE OSMOSIS MEMBRANES AND SUBSTRATE OPTIMIZATION ”, which she prepared after fulfilling the requirements specified in the associated legislations, before the jury whose signatures are below.

Thesis Advisor :	**Prof. Dr. Levent TRABZON** Istanbul Technical University	…….
Co-advisor :	**Asst. Prof. Dr. Çiğdem TAŞDELEN YÜCEDAĞ** Gebze Technical University	.....
Jury Members :	**Assoc. Prof. Dr. Ali KILIÇ** Istanbul Technical University	.....
	Asst. Prof. Dr. Osman EKSİK Gebze Technical University	…….
	Asst. Prof Dr. Canan Gamze GÜLERYÜZ PARASIZ Istanbul Technical University	……

Date of Submission : 03 December 2023
Date of Defense : 02 February 2024

To Türkiye's century,

FOREWORD

During the master's degree process, I would like to thank my supervisor Levent TRABZON and my co-advisors Çiğdem TAŞDELEN YÜCEDAĞ, Ali KILIÇ, and Osman EKSİK for all their support and teaching. I would like to thank my family who always supports me, friends, MEMS Lab family, and TEMAG Lab family, especially Hilal ÖZYURT, for their moral support.

February 2024

Büşra ARSLAN
(Mechanical Enginneer)

TABLE OF CONTENTS

ABBREVIATIONS

FR **:**Feed rate
MPD **:**m-phenylenediamine
Nm **:**Nano meter
NMP **:**N-Methyl-Pyrrolidone
P **:**Pressure
PA **:**Polyamide
PET **:**Polyethilene
PSU **:**Polysulfone
RO **:**Ters ozmoz
T **:**Tempereture
TMC **:**Trimethylene carbonate

LIST OF TABLES

Page

LIST OF FIGURES

Page

POLYAMIDE SYNTHESIS FOR REVERSE OSMOSIS MEMBRANES AND SUBSTRATE OPTIMIZATION

SUMMARY

Because of growing population, global warming and increasing industrialisation, our need for clean water is growing. Water treatment systems can be used to treat industrial wastewater, sewage, etc., as well as sea water, and turn it into drinking water. There are many systems for purifying water. Nanofiltration, microfiltration, reverse osmosis, forward osmosis, and electrodialysis are the most common. 60% of the world's water purification systems are RO. In addition, the use of polymer membrane is common. In general, the RO membranes work under the press, which is able to change the pressure from 60 bar up to 100 bar. Reducing energy consumption is the most issue in RO research due to the high pressure. The cost of RO systems can be reduced by reducing the amount of pressure applied. When the amount of pressure applied is reduced, cost effectiveness is achieved. Reverse osmosis is the process by which water is desalinated using membranes that separate the dissolved components in the feed water but allow the water to pass through. In the reverse osmosis membrane process, as water passes through a membrane by the solution-diffusion mechanism, solutes are retained by electrostatic forces in their size and dissolved ions on the membrane surface. Polymeric RO is composed of three layers. The firs layer, a thin film, which is made up of polyamide separates the components like salt ions. The second layer, a porous polysulfone support layer, directs the flow of water. The final layer, a nonwoven PET layer, increases mechanical strength. Polysulfone carrier layers can be produced by electroblowing, electrospinning or solution blowing. The support layer produced by nanofiber production methods generally has a more porous structure. The nanofiber support layer leads to useful way by which the water flux conveniently pass through, contrast to other support layer types. This results in a high water flow and a reduction in the required applied pressure. This situation reduced energy concuption. The supporting layers made by the phase inversion method have a low percentage of the surface voidand the void size on the surface is relatively small compared to the others support layer types made by nanofiber production methods. The advantage of the phase inversion method is that is more suitable for industrial production. The reasons for the selection of nanofiber production by electro-blow spinning method are that the fiber optimization process is relatively easier and it is also efficient in mass production.

TERS OZMOZ MEMBRANLAR İÇİN POLYAMİD SENTEZİ VE ALTLIK YÜZEYİ OPTİMİZESİ

ÖZET

Büyüyen popülasyon, küresel ısınma ve artan endüstriyelleşme ile birlikte temiz su ihtiyacımız da artmaktadır. Bunun için su arıtma sistemleri ile endüstride kullanılan atık suların, kanalizasyon suları vs arıtıldığı gibi deniz suyu da arıtılarak içme suyuna dönüştürülebilir. Bir cok çeşit su arıtma sistemleri vardır. Nanofiltrasyon, mikrofiltrasyon, düz ozmoz membranlar, elektrodiyaliz ve ters ozmoz membralar bunlardan bazılarıdır. Ters ozmoz membranlar dünyada kullanılan su arıtma sistemlerinin %60'ini oluşturmaktadır. Polimerik membranlar su arıtma sistemlerinde aktif rol oynarlar. Ters ozmoz membranlar yaklasik 60 ile 100 bar arasında değişen yüksek basınçta çalışma aralığına sahiptir. Kullanilan basınç aralığının düşürülmesi tüketilecek enerji miktarını da düşürme eğiliminde olacaktır. Bu durum maliyeti düşürür. Ters osmosis prosesinde, besleme suyunda çözünmüş bileşenleri ayıran ancak suyun içinden akmasını sağlayan membranların kullanılarak suyu tuzdan arındırmak için basınç tahrikli prosedür olarak kabul edilir. Ters Ozmoziz membrane prosesinde su, çözelti-difüzyon mekanizmasıyla bir zar vasıtasıyla geçerken, çözünen maddeler kendi boyutu ve zar yüzeyinin çözünmüş iyonlarda elektrostatik etkileşimleri ile tutulur. Zardan geçen su akısı ve tuz reddi miktarı enerji tüketimi ile beraber iyileştirilmesi gereken iki önemli faktördür. Araştırmalarda su akısı ile tuz reddi arasında bir ters orantı genel olarak gözlenmiştir. Su akısı artması suyun membrane hızlı bir biçimde geçmesine sebep olur. Bu durum suyun içindeki tuz iyonlarının reddini negatif etkiler. İki parametrede optimum değerlere ulaşmak oldukça önemli bir noktadır. Ters ozmoz membranın fiziksel ve kimyasal yapısı tüketilen enerjiyi, su akısını ve tuz reddini doğrudan etkiler. Polimerik ters ozmoz membranlar üç katmandan oluşur. Polyamide ile oluşturulup üst kısımda seçici ultra ince deri polimer tabakası, ana ayırma işlemini yapar. Polysulfondan yapılan orta katman gözeneklidir ve su akışının yolunu kanalize eder. Alt tabaka dokunmamış olup, genellikle PET'den yapılmış olur ve mekanik dayanımı arttırır. Polyamide ince tabaka optimize edilmesi gereken en önemli tabakadır. Polyamide ince tabakanın kalınlığı su akısını negative etkiler. Bunun ile birlikte aromatik polyamide sentezi sırasında amin gruplarını sağlayan MPD monomeri konsantrasyonu artması ile tuz reddi iyileştirilebilir. MPD monomeri oranı artması ile polyamide katmanın kalınlığı değişecektir. Bu ve bir çok sebepten polyamide sentezi optimizasyonu önem arz eder. Polysülfon destekleyici katman elektro eğirme, üflemeli eğirme ve elektrikli üflemeli eğirme ile yapılabilir. Bu yöntemlerle yapılan destekleyici katmanın por oranı çok yüksek olur. Nanolif katmanlarının kullanılması su için daha geniş yollar sağlar. Böylece daha düşük basınçta daha yüksek akı sağlanır. Bu ters osmozda enerji tüketimini azaltacaktır. Phase inversion yöntemi ile yapılan destekleyici tabakalar por oranı düşük olmak ile birlikte por büyüklüğü diğerlerine görece küçüktür. Phase inversion metodunun avantajı ise endüstriyel üretime daha uygun olmasıdır. Elektro-üfleme eğirme yöntemi ile nanolif üretiminin seçilmesinin lif optimizasyonu işleminin görece daha kolay olması ve seri üretimde de verimli olması terhis sebepleri arasındadır. Elektro-üfleme

eğirme ile lif oluşturmak için belirli parametrelere dikkat edilmesi gerekmektedir. Sistem parametreleri, çözelti parametreleri ve çevre parametreleri olmak üzere üç ana faktöre ayrılmaktadır. Sistem parametreleri kapsamında; hava basıncı, besleme hızı ve voltaj değeri optimize edildi. Çözelti parametreleri kapsamında polimerin oranı ilk optimize edildi. Bu süreçte system parametreleri optimize edilmesi ve çözeltinin polimer oranı optimize edilmesi eş zamanlı olarak yapıldı. Sistem parametreleri optimizasyonu tamamlandı ve çözelti optimizasyonuna devam edildi. Başlangıçta DMF çözücü olarak kullanılsa da çözelti optimizasyonu sırasında NMP ve DMF birlikte kullanıldı. NMP ve DMF farklı oranlarda denendi. Polimerin çözünmesine katkı sağladığı kanıtlandı. DMF ve NMP'nin birbirinden farklı kaynama noktalarına sahip olması optimizasyon sırasında NMP kullanılması ikinci avantaj olarak üretime yansıdı. NMP ve DMF oranları değiştirilerek lif oluşumu için optimum kaynama noktası elde edildi. Ortam parametreleri kapsamında nem ve sıcaklık göz önünde bulunduruldu. Ortamın nem oranı lif oluşumu için kurutucu ile dengelendi. Yazın elde edilen sonuçlar kışın farklı ortam koşullarında denendi. Ortam parametrelerini değiştirmesi sebebi ile mevsim lif oluşumunu negative etkileyen bir faktör olsa da çözücü optimizasyonu sayesinde farklı koşullarda da optimum lif atımı elde edildi. Destek katmanın nanolif karakterizasonu SEM görüntü analizi ile yapıldı. Droplet (yüzey üzerinde lif oluşturmamış yuvarlak polimer parçaları) ve lif çapları ImageJ bilgisayar program ile SEM görüntüleri kullanılarak analiz edildi. Droplet çap dağılım grafikleri origin ve excel ile çıkarıldı. Bu dağılımların sonucu ile lif optimizasyonları yapıldı. Elektro-üfleme eğilme parametrelerinin lif çapı dağılımına olan etkileri analiz edildi. Basın. 3 bar dan 4 bara çıktığında lif çapı ortalamasının düştüğü gözlemlendi. Basınç değeri 3.5 bar olduğunda bu orantının bozulduğu gözlemlendi. Besleme hızı azaldıkça ortalama lif çapının azaldığı gözlenmiştir. NMP ve DMF uygun oranda kullanıldığında dropletlerden arınmış bir yüzey elde edildiği gözlemlendi. SEM görüntüleri analizleri dışında lif yapılarının basitçe ve gözle analiz edilebilmesi için yeşil renkli meşler üzerinde lif üretimleri yapıldı. NMP oranı arttıkça çözücünün ıslak attığı, DMF oranının arttıkça is polimerin kuru attığı yani dropletlerin arttığı gözlemlendi. NMP'nin kaynama noktasının DMF'e oranla daha yüksek olması ile NMP oranı arttıkça çözelti buharlaşması zorlandı. DMF oranı arttıkça çözelti lif oluşumundan önce buharlaştı. Erken buharlaşan çözücü polimerin iğne ucunu kısa süreli tıkaması ve droplet sayısının artışı olarak sonuçlandı. Basıncın buharlaşmaya olan etkisi incelendi. Optimum solüsyon parametreleri besleme hızı ve voltaja rağmen 2 bar uyulandığında solüsyonun içerisindeki solvent buharlaşmadı. Por çapları optimize edilmesi için üretimin yarı zamanlı yön değişimi sağlandı. Böylece liflerin konumu birbirine daha çok yaklaştırıldı. Por çapı optimizasyonu için yapılan iki uygulama ise üretim süresinin optimize edilmesi ve sıcak basınç uygulama işlemidir. Sıcak basınç uygulaması sadece por çapına pozitif etkisi yoktur. Por çapı optimizasyonu dışında; elektro-üfleme eğirme yöntemi ile üretilen nanolif altlıkların mekanik dayanımı arttırılması için de sıcak basınç uygulaması yapıldı. Sıcak basınç uygulama işlemi sırasında yüzey porları liflerin genişleyip yan yana gelmeleri ile küçültür. Sıcaklık ve basıncın etkisi ile liflerin dayanımı artar. Sıcak press ile mekanik dayanımı yapılan nanolif destek katmanın yüzey hidrofilikliğinde iyileşme gözlendi. Por büyüklüğü analizi için SEM analizi alınmış destek yüzeyleri ImageJ programı ile analiz edilmiştir. Por yapıları üç boyutlu olduğu için porları temsilen lifler arasında kalan boşluklar ölçülmüş; tek bir boşluk için ölçüm farklı noktalardan ölçüm alınmış ve bir boşluk büyüklüğü için ölçümlerin ortalaması alınmıştır. Yüzeyin SEM görüntüsünde bulunan bütün boşluklar için aynı ölçüm alınmıştır. Yüzey üzerindeki boşluk dağılımları hesaplanmıştır. Bir çok parametre polyamide sentezine etki eder.

Bunlar destek yüzeyin parametreleri ve sentez parametreleri olarak iki temel başlığa ayırılıp; bu parametrelerin poliamid sentezine olan etkileri incelendi. Destek yüzeyin parametreleri şunlar olarak belirlendi: yüzey hidrofilikliği, yüzey hidrofobikliği, polimer etkisi, por çapı oranı, porosity yüzdesi. Sentez parametreleri şu şekilde belirlendi: kürlenme süresi, kürlenme sıcaklığı, MPD konsantrasyonu, TMC konsantrasyonu, MPD temas süresi, TMC temas süresi, çözülerin yoğunluğu, çözücülerin sıcaklığı ve MPD ve TMC nin temas sırası. Substrate yüzeyin hidrofilikliği, por çaplarının optimizasonu direkt olarak poliamid ince tabakanın sentezine etki eden parametrelerdir. Boşluklu yapıların fazla olduğu ve sıcak basınç uygulamasının yapılmadığı destek yüzeylerinde poliamid sentezi görülmedi. Sıcak basınç işlemi ortalama boşluk büyüklüğü ve poliamid sentezinin yüzeyi kaplama oranında göre optimize edildi. Optimum sıcak basınç uygulaması ile poliamidin yüzeyi verimli bir şekilde kapladığı SEM görüntüleri ile gözlemlendi. Poliamid sentezi FTIR sonuçları ile doğrulandı.

1.INTRODUCTION

1.1 Purpose of Thesis

The main aim of the thesis is the production of thin-film polaymide composite mebrane that can be used in reverse osmosis systems. Within the scope of the thesis, the nanofiber substrate surface was obtained using solution-blowing and electro-blowing. The optimization of the substrate surface was performed in two stages. Firstly, nanofiber optimization and secondly, average void size on the surface optimization of the substrate surface were performed by utilizing hot-press. The experiments show that surface hydrophobicity and void size on the surface increase negatively affected polyamide synthesis, as a result substrate surface optimization was performed in order to perform polyamide synthesis efficiently. According to experiments hot-press treatment improved void size on the surface reduction and superhydrophobic surface property.

1.2 Literature Review

1.2.1 Nanofiber substrate structure and nanofibers

Nanomaterials are categorized into zero-dimensional, one dimensional, two dimensional, and three- dimensional forms. The classification of nanomaterials according to size is depicted in the Figure1.1. One-dimensional nanomaterials are comprised of up of nanofibers and nanowires, whereas zero-dimensional nanomaterials are composed of metal nanoparticles and quantum dots. Graphene sheets and thin films are examples of two-dimensional nanomaterials, while liposomes are instances of three-dimensional nanomaterials [1].

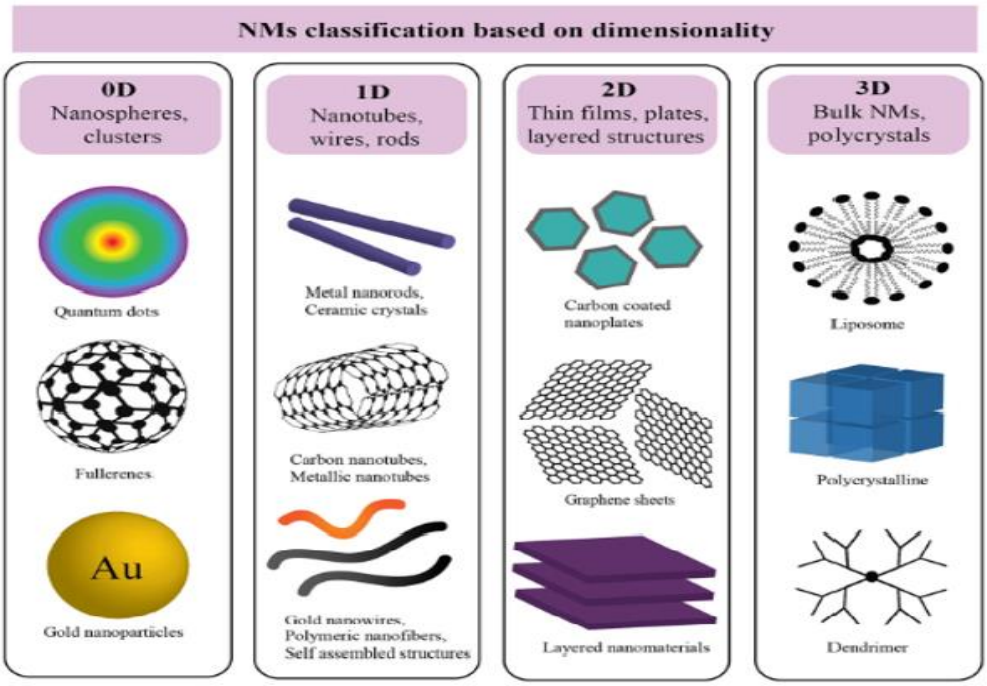

Figure 1.1: Nanomaterials classification based on dimensionallyt [1].

Since nanofibers have diameters of 1000 nm or less, they are categorized as one-dimensional structures [2]. There are numerous methods for producing nanofibers, as depending on their application and cost-efectiveness. Additionally, articles highlight solution blowing, electro blowing, phase inversion, template synthesis, and self-asSEMbly as noteworthy methods. The most common method is electrospinning. Both nanofiber and dense membrane substrate structures can be used for reverse osmosis membranes [3]. Nanofibers create a high percentage of the surface voidsubstrate structure, allowing for increased permability [4].

1.2.2 Nanofiber production techniques

1.2.2.1 Working princible

In 1964, Sir Goeffrey Taylor conducted an examination involving a small volume of liquid subjected to a high electrical field. The small liquid volume transformed into a conical shape with a 49.3^{o} angle, progressively becoming thinner over time, and exhibiting a helical motion. When similar shape is applied with a polymer solution, it resulted in the formation of a Taylor cone and a helical motion [5] (Fig. 1.2). Under appropriate parameters, nanofibers are generated in conjunction with the phenomenon of solvent evaporation.

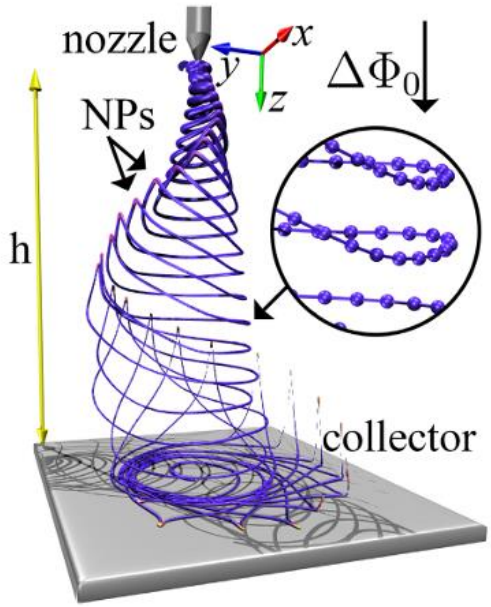

Figure 1.2: Illustration of nanofiber formation [34].

The Figure 1.3 shows how repulsive forces overcome the surface tension on the droplet to form a Taylor cone [5]. These forces cause the cone to become thinner and move randomly. The evaporation of a solution forms nanofibers

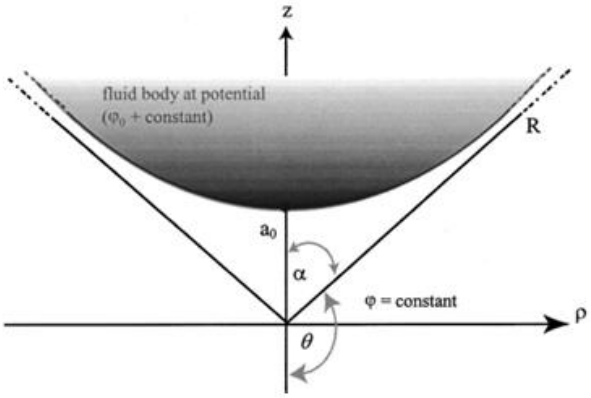

Figure 1.3: Taylor Cone [5].

1.2.2.2 Electrospinning

Electrospinning is a popular technique for forming nanofibers from organic and inorganic materials. Multistage processes are used to produce inorganic nanofibers. Polymers, as organic materials, can easily be converted into nanofibers by adjusting electrospinning parameters. Electrospinning devices can also be used to adjust nanofiber diameter and void size on the surface. However, it has some disadvantages, such as the usage of hazardous solvents. The cost of solvents may increase the cost of

an electrospinning system because majority of the polymer solution is consist of solvent itself. Furthermore, the system is intrinsically inaccuracy for mass production [6-7]. Electrospinning system consist of a syringe pump, a collector, a voltage source, and a needle. Electrospinning creates nanofibers by utilizing electrostatic forces. The voltage is effecting the surface tension of polymer solution, and forming the Taylor's cone and polymer molecules alignment The solvent component evaporates at the right time, resulting in the production of nanofibers. To optimize the morphology of the nanofibers, voltage, feed rate, and collector-needle distance are used.

1.2.2.3 Electroblowing

Similar to the solution blowing method, electroblowing employs a nozzle, a syringe pump, and an air pressure system (Fig. 1.4). Nevertheless, a pivotal differentiation exist between electro-blowing and solution blowing. Air pressure play the role of the driving force in the solution blowing process, whereas the electro-blowing system relies on both air pressure and electrostatic forces. This dual driving force characteristic gives the electro-blowing a substantial advantage. This situation combines techniques of electro-spinning and solution blowing.

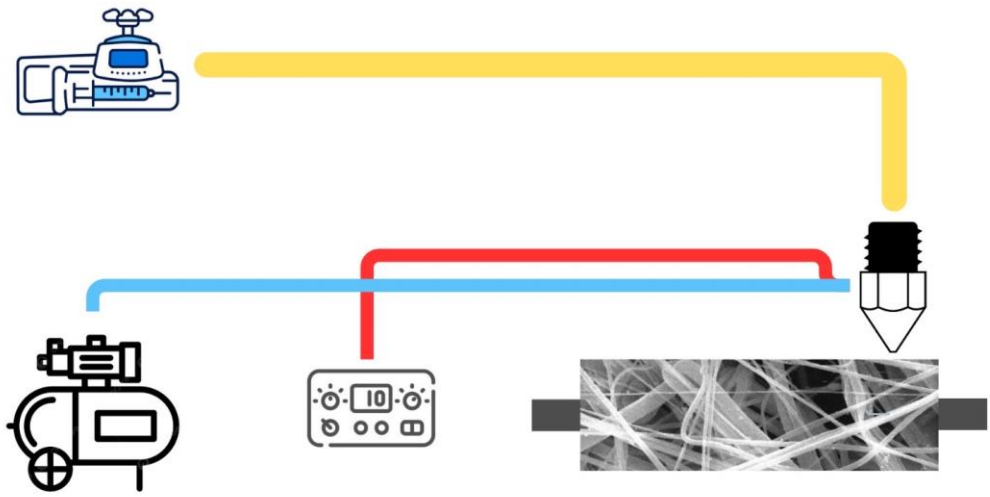

Figure 1.4: Electroblowing system template.

1.2.2.4 Solution blowing

Solution Blowing systems generally involve collector, neddle, nozzle, pressure system, and homogenizer (Figure 1.5). Pressure is utilized as a driving force. Pressure

is directed at a certain angle determined by the geometry of the nozzle. When the polymer solution is exposed to pressure, Taylor's cone develops, molecule chains gradually align one after another in time. When the solvent evaporation occurs at the ideal time, nanofibers are produced. The solution blowing process is depicted in the Figure 1.5. Comparing the percentage of the surface voidrate of the same polymers produced by solution blowing spinning and electrospinning, the solution blowing spinning method produced a range of 75%-95%, while the electrospinning produced a percentage of the surface voidrate of 67%. Solution blowing has higher (75-95%) percentage of the surface voidratio In comparing to electrospinning method (67%). Pore size in solution blowing spinning and electrospinning productions was compared in the study. The findings demonstrated that pore size is 3 μm in electrospinning and it was found 8–17 μm in solution blowing [8].

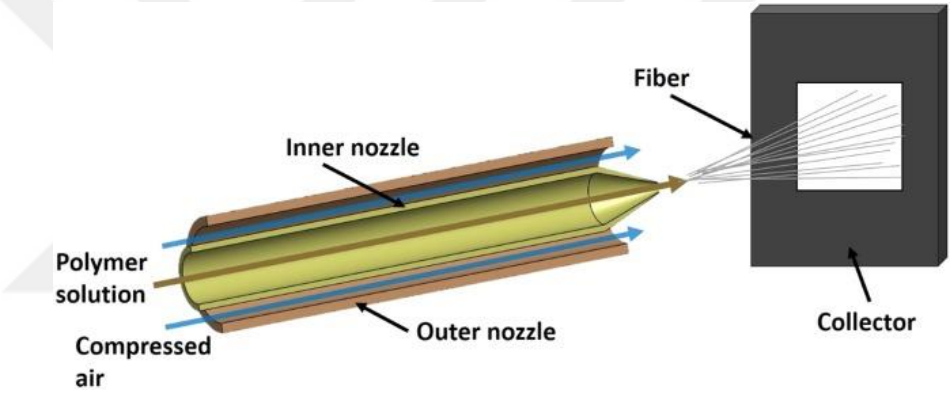

Figure 1.5: Solutionblowing system template [35].

1.2.2.5 Electro-blowing parameters for nanofiber formation

Fiber formation parameters include system parameters, solution parameters and ambient parameters [9] (Fig. 1.6). Each type of parameter is discussed in detail to optimise fiber formation. System parameters consist of solution feed rate, voltage, nozzle geometry, distance between collector and nozzle, collector rotation rate. On the other hand, air pressure and voltage are the two most important components of the system parameters. As the feed rises, the diameter of the fiber increases. As the voltage increases, the surface tension is overcome in a way that is comfortable for soluion with a high viscosity. The formation of polymer jets is facilitated by electrostatic forces. In addition, high voltage allows the fiber to stretch and elongate more, resulting in a thinner fiber diameter [10]. Air pressure has a significant impact on fiber production,

including facilitating convenient evaporation [11]. Additionally, similar to voltage, air pressure results in a decrease in fiber diameter [12]. The air pressure helps the surface tension to form the Taylor cone by weakeing the flow of the polymer solution and pushing the flow forward. Therefore increasing air pressure, obtaining more thinner fiber diameter. According to a study, if the air pressure exceeds the optimum level, the fiber will break off at thinner diameter than the normal range. Thus, it was observed that these very thin fibers were entangled and scattered around [13]. The solution parameters include viscosity, molecular weight, chain lenght, boiling pressure of the solvent, diectric properties, solubulity, concentration of the solution temperature of the solution and, surface tension. Molecular weight and chain lenght, concentration of the solution are interrelated. Molecul chains entangled when fiber formation situation and these chains form fiber. However, if the length of the chain is very short, it can be insufficient to produce fiber. Furthermore, concentration effects on surface tension and viscosity. Increasing the concentration of a solution results in a rise in viscosity and surface tension [14]. The ambient parameters include temperature and humudity. The evaporation of solvents is influenced by temperature and humidity [15].

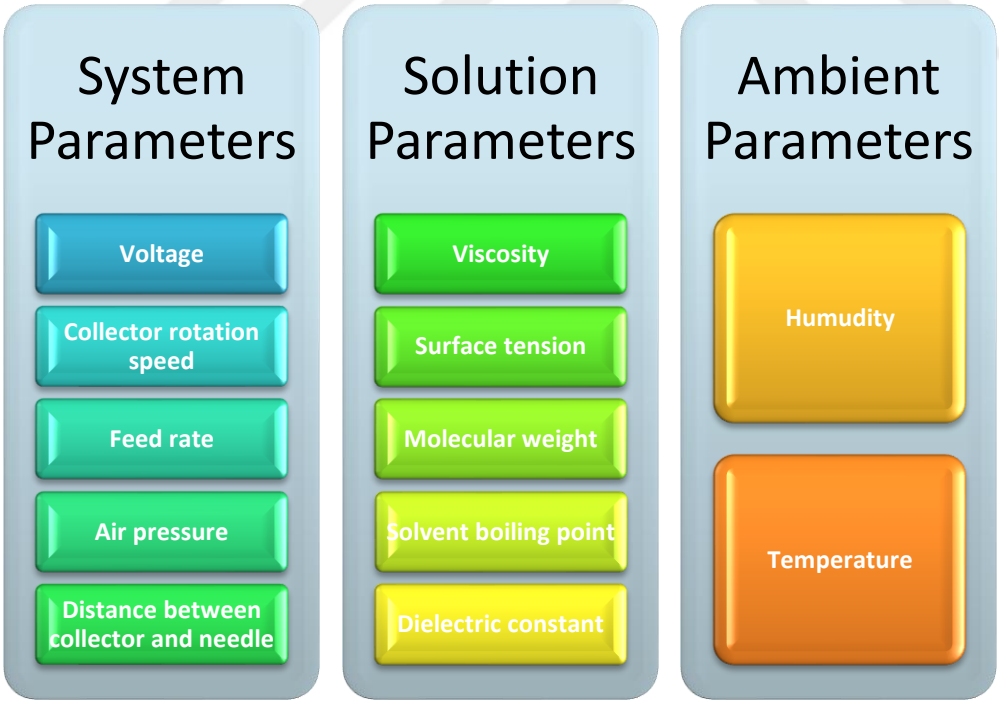

Figure1.6 : Parameters of electroblowing.

1.2.2.6 Phase inversion

Phase inversion is used to create dense membrane structures, and it is suitable for mass production due to its simple mechanism and inherent stability. After preparing the polymer solution under the determined optimum conditions, it is cast onto a glass surface. This phenomenon takes place when the solvent in the casting polymer solution dissolves in the coagulation bath and separates from the polymer structure. Therefore, a porous structure is produced. Pores are then created as a result of the bubbles formed when the solvent moves away from the polymer solution. In order to modify the pore dimensions, percentage of the surface voidpercentage, and chemical properties of the hydrophilic surface, specific parameters can be adjusted. The void size on the surface is influenced by the solvents used, concentration of the solution, and components of the pore former. When PEG polymer is added into the polymer solution, larger pore surfaces are formed, and it dissolves together with the solvent in the coagulation bath. When PEG dissolves in the coagulation bath, it leaves hydrophilic groups on the substrate surface [16]. This situation increases the hydrophilic property of the substrate surface. The temperature of the coagulation bath, the concentration of polymers, the thickness of the doctor blade is casting are other parameters that determine the pore structure [17].

1.2.3 Void size on the surface optimization techniques of nanofiber substrate

Electrospinning methods can create three-dimensional flufy structures. Although nanofiber structures provide us with high porosity, pore size should be optimised with different methods. Studies have shown that the void size should be 450 nm and below for polyamide synthesis and strength of polyamide thin film [18]. When the substrates produced with nanofibers are taken into consideration the strength of the structure and the parameters affecting the polymerization, various improvement methods are used. When the substrates produced with nanofibers are taken into consideration the strength of the structure and the parameters affecting the polymerization, various improvement methods are used [19]. Heat treatment, sintering, and hot-press are among these methods. Hot pressing is a process in which pressure is applied at a specific temperature using a device. This causes the nanofibers to flatten, reducing their diameters, and the spongy structure becomes thinner. The hardness of the substrate surface changes with heat treatment and pressure. Nanomaterials can be used for active

layer and substrate membrane. Thus, hot-pressing will optimize both the flufy structure and the pore size by reducing the pore size [20].

1.2.4 Use of nanomaterials in reverse osmosis membranes

Applications of nanomaterials in membrane technology are numerous. Nano particles enhance the membrane's ability to reject salt and increase water permeability by modifying the surface' toughness and hydrophilicity. Graphene oxide, graphene quantum dot, CNT and TiO2 are all frequently utilized nanomaterials in water purification technology [20-21]. Nanofibers vary in how they affect surface morphology depending on the size and concentration. The layer size of graphene oxide get smaller lead to that the influence of graphene oxide on surface morphology change as more hydrophilic maker. As the graphene oxide size decreases, the surface area graphene oxide increases, and more hydrophilic groups are placed around it. Therefore, graphene oxide can interact more with water molecules [22].

1.2.4 Polyamide thin film and thin film composite

Thin film composite made of non-woven, support layer and polyamide thin film. Salt and water are separated by a polyamide thin film with a cross-linked aromatic structures (Fig. 1.7). Two monomers containing acyl chloride and amine groups dissolved in immiscible phases: m-phenylenediamine (MPD) or piperazine (PIP) dissolved in water and trimesoyl chloride (TMC) dissolved in organic phase (e.g. hexane,heptane) (Fig. 1.8). With the positive effect of the in solubility of the TMC monomer in water, the MPD monomers diffuse towards the organic solution. While MPD diffusion is initially fast, the rate of diffusion decreases with time. With the effect of the polymer synthesis at the interface, the MPD diffusion and reaction stops [23]. The parameters affecting the synthesis of polyamide are demonstrated in the Fig. 1.8. Production methods are generally by contacting the MPD-water solution and TMC-organic solution with the support layer respectively. Solutions the main influencing factor is the density of the solution. The high density solution should be contracted. However, there is no single method. The methods in Fig. 1.7 are some of the is

methods. Properties of polyamide thin film including crossling-degree, toughness, hydrophilicity and tickness affect on water flux and salt rejection [24-25].

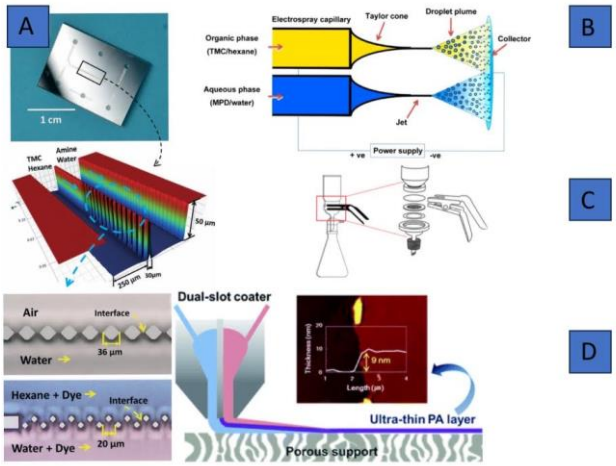

Figure 1 7: Production methods of polyamide(A) [36] Microfluidic method, (B) Electrospray method [37], (C) Vacuum filtration method [24], (D) Dual-slot coated method [25].

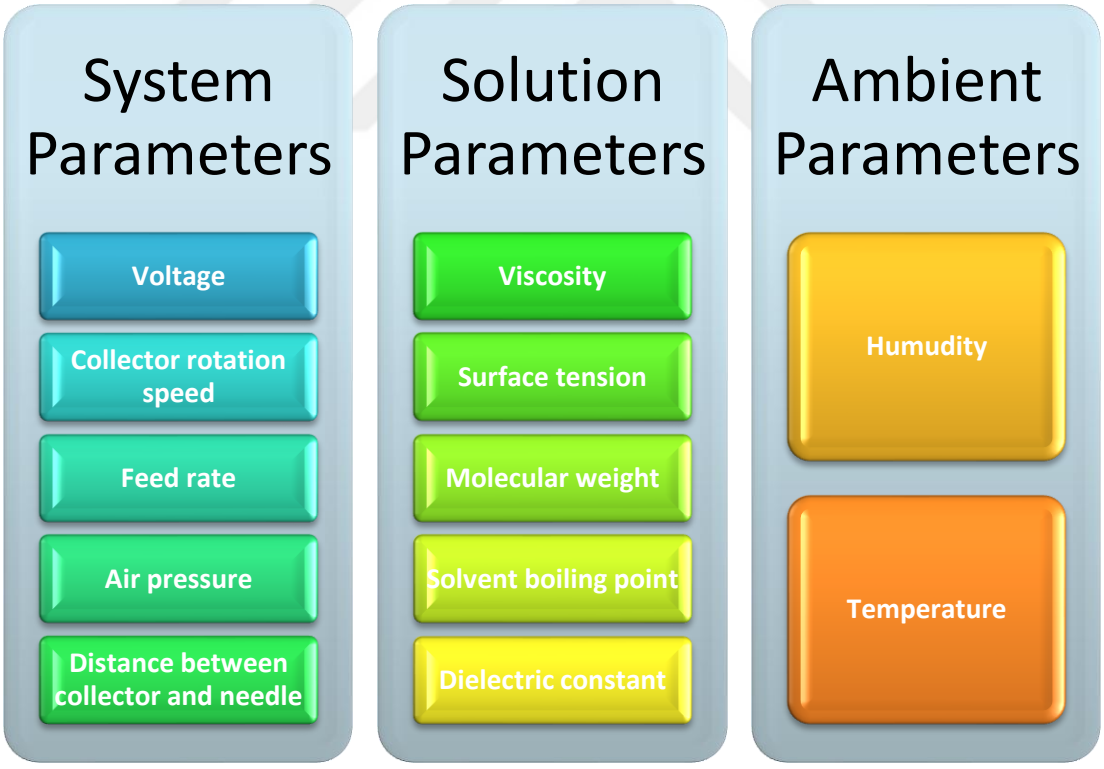

Figure 1.8: Parameters of polyamide synthesis.

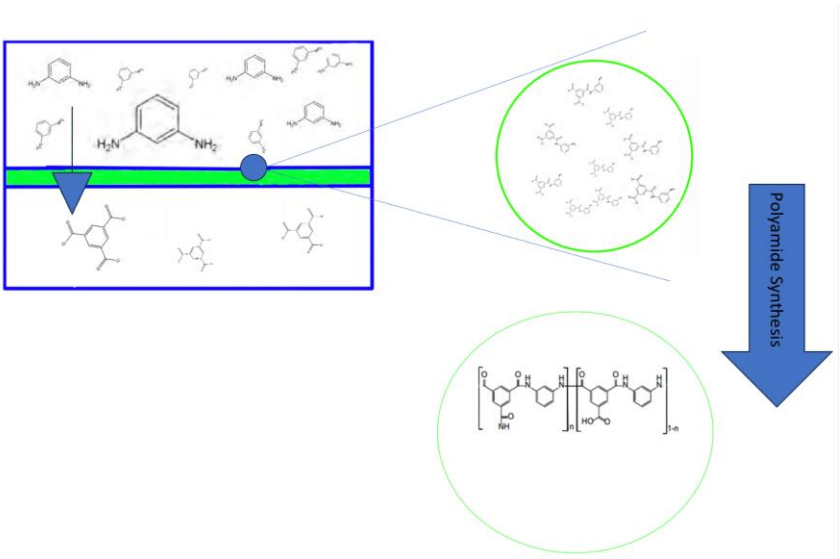

Figure 1.9: Polyamise synthesis process.

1.3 Hypothesis

In this thesis, it is aimed at increasing the percentage of the surface void by thinning the fibers with the electroblow production method. This machine was used during production. The effect of solution parameters on fiber optimization in the electro-blowing system was predicted and proven. In addition, it was observed that the average void size on the surface and surface hydrophilicity should be optimized in order for the produced substrate surface to be suitable for polyamide synthesis, and polyamide synthesis was successfully performed and proved by optimizing it with the hot press treatment method.

2. MATERIALS &METHOD

2.1 Nanofiber Substrate Optimization and Production

Due to its exceptional mechanical, chemical and thermal qualities, polysulfone is a polymer frequently preferred in the production of membranes and nanofibers Polysulfone was dissolved by utilising dimethyl formamide (DMF) and methyl prolodone (NMP) as a organic solvent. The polysulphone utilized possesses an average molecular mass of 35,000 daltons. The chemical materials used possess analytical purity. Nanofiber produce on commercial non-woven. The nanofiber production and nanofiber optimization were made by AREKA® miniaero machine. Optimization of void size on surface was made by hydrolic hot press machine. Nanofiber optimization and void size on the surface optimization of resulting substrate layer were characterized by SEM, and contact angle.

2.1.1Nanofiber production and optimization

2.1.1.1 Solution optimization

The initial step was to establish the correct concentration of both the solvents and polymers employed. Various polysulfone concentrations were initially tested, as presented in the table, prior to observing the nanofibers within the electro-blowing system. In this step, only N, N-Dimethylformamide was utilized as a solvent.

The proper concentration of polysulfone in the DMF solvent was determined after SEM image analyses and observing the spun material on the green mesh. After determining the concentration of polysulfone, identifying the optimal solvent type and ratio utilized, as specified in the table A.1 (in the appendix). Second state, two different solvents, DMF and NMP, were tested at varying ratios.

Table 2.2: Properties of solution.

Propoties	NMP	DMF
Chemical Formula	C5H9NO	C3H7NO
Density g/cm3	1.034	0.9445
Molar Mass g/mol	99.13	73.095
Purity%	99.00-extra pure	99.00-extra pure
Viscosity mPa.s	1.65	0.92
Dielectric Constant	32.2	36.7
Boiling Point	204	155
Solunility in Water	Yes	Yes
Yüzey Gerilimi N/m	40.70	37.10

T**able 2.3:** Experimental groups of solvent optimization.

Exp. Group	Conc. (%wt.)	Solvent	P (Bar)	FR (ml/h)	V (V)
S9	%25	%90 DMF-%10NMP	3	5	20
S10	%25	%80DMF-%20NMP	3	5	20
S11	%25	%70DMF-%30NMP	3	5	20
S12	%25	%60DMF-%40NMP	3	5	20
S13	%25	%50DMF-%50NMP	3	5	20

2.1.1.2 Electro-blowing parameters for optimization

The second step was to establish the correct parameters of electro-blowing system parameters. Fundamental electro-blowing parameters are pumping rate, air pressure, and voltage. The initial, air pressure as driving force tested with different pumping rates, as specified in the table . After determining the optimal air pressure, the voltage values are evaluated at various pumping rates, as specified in the table.

2.2 Percentage of The Surface Voidof Substrate Layer Optimization

The substrate surface's mechanical strength, void size on the surface, and percentage of the surface voidratio have been optimised. For optimisation, production was carried out at three different periots: 40 minutes, 60 minutes and 120 minutes respectively. To optimise the void structure during production, half of the production was carried out in the specified direction and the remainder of the production was carried out by rotating the non-woven 90 degrees, as seen shown in the Figure 2.1.

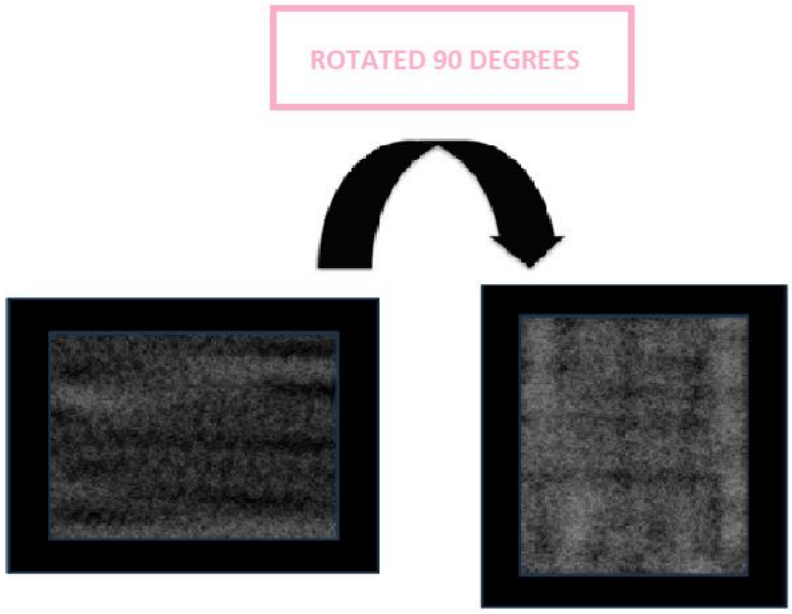

Figure 2.1: Rotation of the substra surface during production.

The void of the surface structure and mechanical strength of the substrate surface are optimised by hot press. In order to optimise, hot pressing was carried out at different temperatures, pressures and times as shown in the table 2.4. Owing to its high glass transition temperature (Tg) value teflon is suitable for temperature testing in wide ranges. For the same reason,teflon was used as a protective surface while hot-pressing. The substrate surface was placed between the protective teflon surfaces and experiments were carried out.

Table 2.4: Hot-press treatment optimization experiments.

Experimental Group	Temperature Degree	Pressure (Bar)	Time (Min.)
HT40DK1	70	5	5
HT40DK2	70	5	5
HT40DK3	70	5	5
H40DKT4	70	5	10
HT40DK5	70	5	10
HT40DK6	70	5	10
HT40DK7	70	7	5

Table 2.4 continued

Experimental Group	Temperature Degree	Pressure (Bar)	Time (Min.)
HT40DK8	70	7	5
H40DKT9	70	7	5
HT40DK10	70	7	10
HT40DK11	70	7	10
HT40DK12	70	7	10
HT60DK13	70	5	5
HT60DK14	70	5	5
HT60DK15	70	5	5
HT60DK16	70	5	10
HT60DK17	70	5	10
HT60DK18	70	5	10
HT60DK19	70	7	5
HT60DK20	70	7	5
HT60DK21	70	7	5
HT60DK22	70	7	10
HT60DK23	70	7	10
HT60DK24	70	7	10

Table 2.4 continued

Experimental Group	Temperature Degree	Pressure (Bar)	Time (Min.)
HT120DK25	70	5	5
HT120DK26	70	5	5
HT120DK27	70	5	5
HT120DK28	70	5	10
HT120DK29	70	5	10
HT120DK30	70	5	10
HT120DK31	70	7	5
HT120DK32	70	7	5
HT120DK33	70	7	5
HT120DK34	70	7	10
HT120DK35	70	7	10
HT120DK36	70	7	10

2.3 PolyamideThin Film Synthesis

The synthesis of polyamide was carried out by sequentially pouring monomer solutions onto the substrate surface placed in vacuum filtration. In the first test group, the aqueous MPD solution was first poured onto three different substrate surfaces that had not undergone hot-pressed. The excess MPD aqueous solution on the surface was removed with a glass roller. TMC organic solution is added to the substrate surface impregnated with MPD aqueous solution. The substrate surface was held in an oven at 70^{o}C for 5 minutes to cure. The holding durations of the monomer solutions on the substrate surface were in the ranges shown in the table 2.5. The optimal substrate surfaces were identified through hot press optimization, based on SEM images. Subsequently, polymerization was conducted on these surfaces using experimental parameters documented in the table 2.6, table 2.7 and table 2.8. In the third experimental group, the addition order of TMC organic solution and MPD aqueous

solution to the substrate surface was altered. Firstly, TMC organic solutions were added, followed by MPD aqueous solutions. The third experimental group was completed with the parameters presented in the table.

Table 2.5: Properties of monomer solutions.

Propoties	MPD Solution	TMC Solution
Density g/cm3	1 g/cm3	
Solvent	DI Water	Hexan
Concentration	5 %	0.05 %

Table 2.6: Polyamide synthesis experiment groups.

Sample	TMC Exposure Time (Minutes)	MPD Exposure Time (Minutes)	Oven Temperature (Degree)	Curing Time (Minutes)
NPHT1	3	20	70	5
NPHT2	3	20	70	5
NPHT3	3	20	70	5
NPHT4	1.5	3	70	5
NPHT5	1.5	3	70	5
NPHT6	1.5	3	70	5
NPHT7	1	3	70	5
NPHT8	1	3	70	5
NPHT9	1	3	70	5
NPHT10	1.5	20	70	5
NPHT11	1.5	20	70	5
NPHT12	1.5	20	70	5
NPHT13	1	20	70	5
NPHT14	1	20	70	5
NPHT15	1	20	70	5

Table 2.7:Polyamide synthesis experiment groups 2.

Sample	TMC Exposure Time (Minutes)	MPD Exposure Time (Minutes)	Oven Temperature (Degree)	Time (Minutes)	First Monomer	Hydrophilic Surface Position
NHT16	3	20	70	5	TMC	Hydrohilic Surface on Top
NHT17	3	20	70	5	MPD	Hydrophilic Surface at the Bottom
NHT18	3	20	70	5	MPD	Hydrophilic Surface on Top
NHT19	3	20	70	5	TMC	Hydrophilic Surface at the Bottom

Table 2.8: Polyamide experimental group 3.1.

Experimental Grup	Hot-Press Sample No	TMC Exposure Time	MPD Exposure Time	Curing Temperature	Curing Time (Minutes)
PHT7	HT40DK1	3	20	70	5
PHT8	HT40DK2	3	20	70	5
PHT9	HT40DK3	3	20	70	5
PHT10	HT40DK4	3	20	70	5
PHT11	HT40DK5	3	20	70	5
PHT12	HT40DK6	3	20	70	5
PHT13	HT40DK7	3	20	70	5
PHT14	HT40DK8	3	20	70	5
PHT15	HT40DK9	3	20	70	5
PHT16	HT40DK10	3	20	70	5
PHT17	HT40DK11	3	20	70	5
PHT18	HT40DK12	3	20	70	5
PHT19	HT60DK13	3	20	70	5
PHT20	HT60DK14	3	20	70	5
PHT21	HT60DK15	3	20	70	5
PHT22	HT60DK16	3	20	70	5
PHT23	HT60DK17	3	20	70	5
PHT24	HT60DK18	3	20	70	5
PHT25	HT60DK19	3	20	70	5
PHT26	HT60DK20	3	20	70	5
PHT27	HT60DK21	3	20	70	5
PHT28	HT60DK22	3	20	70	5
PHT29	HT60DK23	3	20	70	5
PHT30	HT60DK24	3	20	70	5
PHT31	HT120DK25	3	20	70	5
PHT32	HT120DK26	3	20	70	5
PHT33	HT120DK27	3	20	70	5
PHT34	HT120DK28	3	20	70	5
PHT35	HT120DK29	3	20	70	5
PHT36	HT120DK30	3	20	70	5
PHT37	HT120DK31	3	20	70	5
PHT38	HT120DK32	3	20	70	5
PHT39	HT120DK33	3	20	70	5
PHT40	HT120DK34	3	20	70	5
PHT41	HT120DK35	3	20	70	5
PHT42	HT120DK36	3	20	70	5
PHT32	HT120DK26	3	20	70	5
PHT33	HT120DK27	3	20	70	5
PHT34	HT120DK28	3	20	70	5
PHT35	HT120DK29	3	20	70	5
PHT36	HT120DK30	3	20	70	5
PHT37	HT120DK31	3	20	70	5
PHT38	HT120DK32	3	20	70	5
PHT39	HT120DK33	3	20	70	5

2.3 Production Devices and Characterization Devices

2.3.1 Nanofiber production machine

The nanofiber nets were produced using the Aerospinner machine, manufactured by Areka Filtration Technologies Ltd. (Fig. 2.2).

Figure 2.2: Aerospinner.

The machine is suitable for both solution blowing and electroblowing and is equipped with an air pressure system connected to a compressed air tank, voltage source, collector with vacuum, homogenizator, syringe pomp, nozzle. The collector can rotates and has a length of 30 cm and a diameter of 10 cm. This provides for the gathering of an independent nanofiber network of 20 cm x 30 cm on the collector, which allows the use of the electroblowing device. nanofiber network of 20 cm x 30 cm on the collector, which allows the use of the electroblowing device.

2.3.2 Scanning electron microscopy

Diameter of nanofiber analysis and void size on the surface analysis were made by utilizing The TESCAN VEGA 3 SEM device. To improve conductivity, an Au/Pd coating was applied to the surface for 165 seconds. Seconds. SEM images anayze with Image J software.

2.3.3 Contact angle

The hydrophilic and hydrophobic properties of the substrate surfaces and polyamide thin film surface were evaluated using contact angle results. Contact angle values were measured using a Theta Lite contact angle meter. The measurement involved pouring 5 microlitres of DI water and measuring the angle between the water drop and the surface.

Figure 2.3: Contact angle measurement.

2.3.4 FT-IR

The polyamide thin film formation was investigated by utilizing the FT-IR analysis method. The specific peaks of the polyamide thin film were observed through the FT-IR analysis method.

3. RESULT AND DISCUSSION

3.1 Polysulfone Nanofiber Optimization for Substrate Structure via Electro-Blowing

3.1.1 Determined optimum parameters of working electro-blowing

Polysulfone nanofiber substrate structure was made with electro-blowing system. Parameters of optimum working conditions for electro-blowing were determined with three main factors. System parameters, solution parameters and prosess parameters were determined and tested in different design of experiment tables. The solution parameters and system parameters such as feed rate, air pressure, etc. were examined on the SEM and green mesh and the fiber images were examined and compared with the researches and the parameters were changed to find the optimum points.

Concentration variation, different solvents and their ratio were varied within the scope of solution parameters. Here, according to the researches, it was observed that concentration is an important effect for the formation of certain chain lengths depending on the molecular weight. Firstly, the polysulfone concentration was increased until fiber formation was observed. DMF solvent was used until the minimum concentration at which fiber formation was observed. Fiber formation was observed at 18 percent polysulfone concentration. The concentration was increased up to 25 percent. At first, as the concentration increased, the solubility of DMF was insufficient and the solution was left to dissolve for one fay and dissolved for two days at night. Fewer droplets were observed when dissolved for two days. NMP solvent was added and the solution was continued to dissolve for one day.

NMP and DMF have different evaporation points. The evaporation point of NMP is 204 degrees while DMF is 155 degrees. Evaporation points of the solvent are very important for fiber formation. Depending on the evaporation points, solvents get rid of the solution and form fibers. Different solvents can be used to evaporate the solvent and get rid of the solution, the distance between the noozle and collector can be changed, or production can be done at different humidity and temperature. Due to the high moisture content, the dryer and electro-blowing device are heated, and the solvent

evaporates more easily. The distance between the noozle and the collector is kept constant. The distance is 30 cm between the noozle and the collector for the machine used. To change the point at which the solvent evaporates, we varied the use of NMP and DMF. NMP is a solvent with a high evaporation point and thus difficult to evaporate. As the volume increase of NMP in the solution, which is difficult to evaporate, beadings were observed more. As the DMF ratio increased, the solvent left the solution before the fiber formation. However, this has also increased the droplet formation. The optimal solvent ratio was found to be 60 per cent DMF and 40 per cent NMP as shown the table 3.1.

Table 3.1: Optimize solution parameters.

Cons. of PSU (% wt.)	Dissolution Temperature	Solvent Ratio	Dissolution Time
% 25	70	%60DMF-%40NMP	24 h

Voltage and compressed air were used as driving forces in the electro-blowing system to overcome the surface tension and form the Taylor cone [26-28]. Air pressure and voltage were tested at different values and their effects on fibers were examined. With the increase in air pressure, the solution flow weakens and the solvent evaporation becomes easier. Air pressure at 2, 3, 3.5 and 4 bar levels were tried respectively. At pressures of 3 bar, 3.5 bar and 4 bar nanofibers were seen, however they were not achievable at 2 bar. Applying 4 bars of pressure resulted in an increase in the quantity of droplets. As air pressure increased, the solution more easily expelled solvent and formed fibers. Surface tension and viscosity increased with concentration, and with these increases, the shear forces created by air pressure were inadequate to form a Taylor cone. Electrostatic forces generated by a voltage are able to overcome surface tension, making it simple to convert the polymer solution into fiber form. 20 kV was determined to be the appropriate voltage.

During the trials, it was observed that it threw wet at low feed rates. In addition to this, it has been observed in the literature that as the feed rate increases; fiber diameters increase due to more polymer molecules coming together to form fibers. However, considering the small average void size on the surface and high percentage of the surface voidratio, it was decided that this would not negatively affect the substrate surface. When 5 and 7 ml/h feed rates were tried, the optimum result was obtained

with 5 ml/h. 7 ml/h feed rate is the production of thicker substrate surface in a short time as it will throw more polymer solution per unit time. Furhermore, selecting a feeding rate of 7 ml/h resulted in an increase in nanofiber diameter. Parameters in the Table 3.2 were determined as optimal parameters

The productions were performed in three time period groups as 40 minutes, 60 minutes, and 120 minutes. Halfway through each production, the non-woven was rotated 90 degrees. Thus, it was aimed to reduce void on the surface structure.

Table 3.2: Optimize production parameters.

Experimental Group	Concentration of PSU (%wt.)	Solvent	Pressure (Bar)	FD (ml/h)	Voltage (V)
S13	%25	%60DMF-%50NMP	4	7	20

3.2 SEM Analysis of Samples

Each of the other details remain the same, except the sample in Figure 3.1.A was prepared overnight, and the sample in Figure 3.1.B was prepared over two days. Figure 3.1.A exhibits droplets, whereas Figure 3.1.B, which has fewer beads, shows no droplets at all. The reason for this variance is because, despite the solution's apparent homogeneity, it is known that the polymer chains are not open.

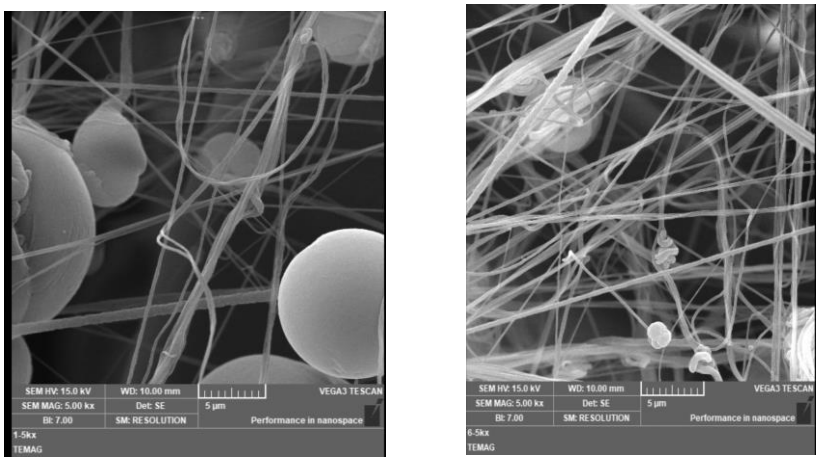

Figure 3.1: (A) Result of the solution prepared overnight (B) Result of the solution prepared for two days.

After two days of stirring the solution, there was an improvement in dissolution and a discernible decrease in the quantity of droplets. To enhance dissolving, an additional solvent was added. The nanofiber diameter distribution of the solution mixed with DMF for one day is shown in Figure 3.2.

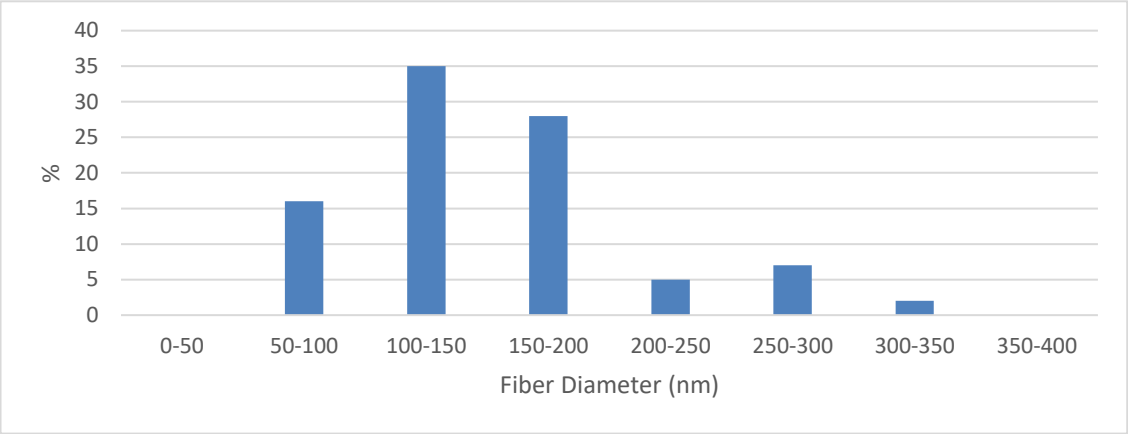

Figure 3.2: The nanofiber diameter distribution of the soluion mixed with DMF for one day.

Twenty percent concentration and 7 ml/h feed rate was used to create the production shown in Figure 3.3 to Figure 3.5. Dimethylformamide (DMF) was added as solvent. The feed rate was 7 ml/h . The diameters of the droplets were decreased as with the pressure drop. , the percentage of the substrate surface area that the droplets covered was computed by ImageJ. The area that the droplets covered on the substrate surface reduced in combination with the applied air pressure. As a result, the optimal air pressure for the investigations was found at 3 bar air pressure level

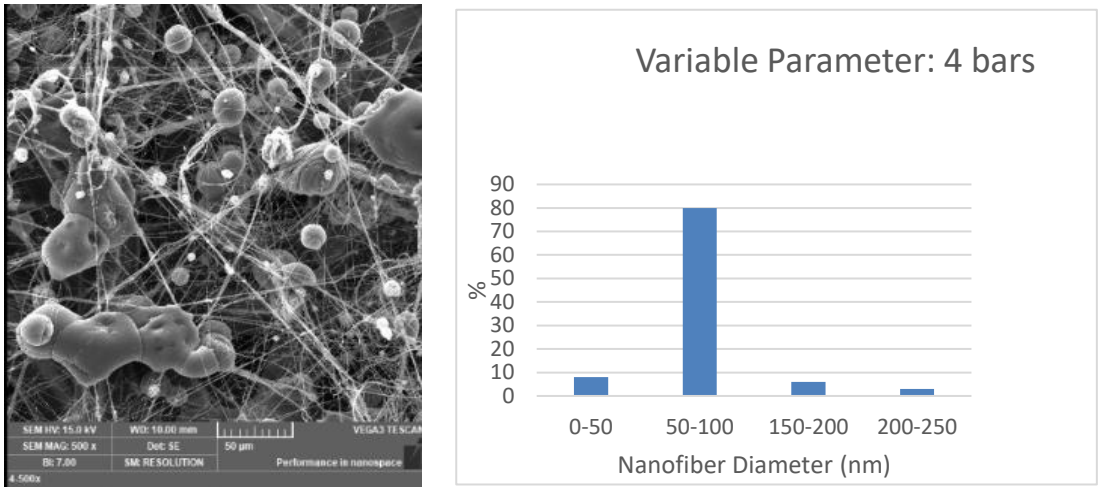

Figure 3.3: (A) SEM images of the sample produced with 5 ml/h, 4 bars, %20 PSU/DMF. (B) Nanofiber diameter distribution.

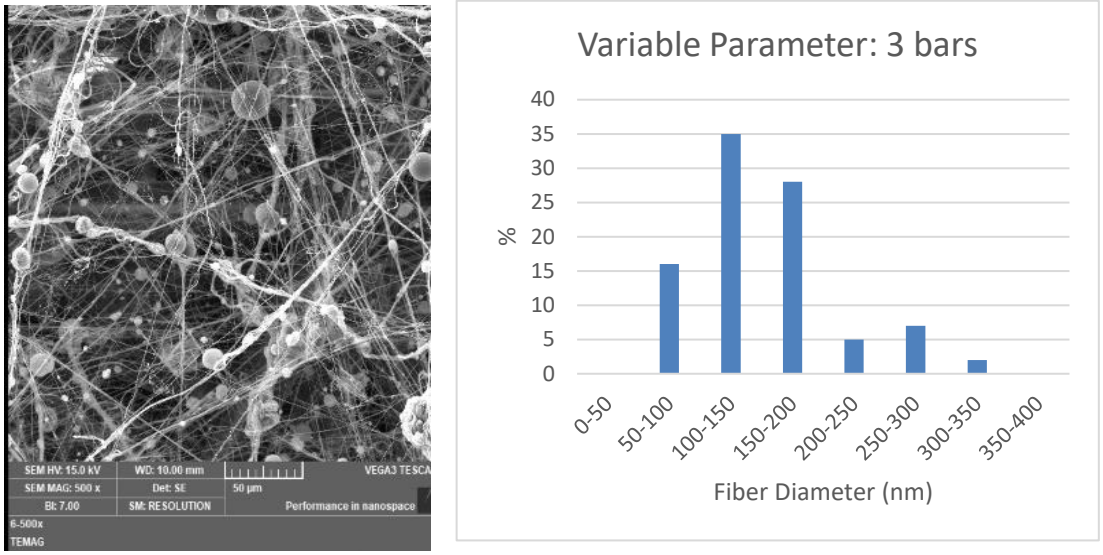

Figure 3.4: (A) SEM image of the sample produced with 5 ml/h, 3 bars, %20 **PSU/DMF, (B) Nanofiber tdiameter disribution.**

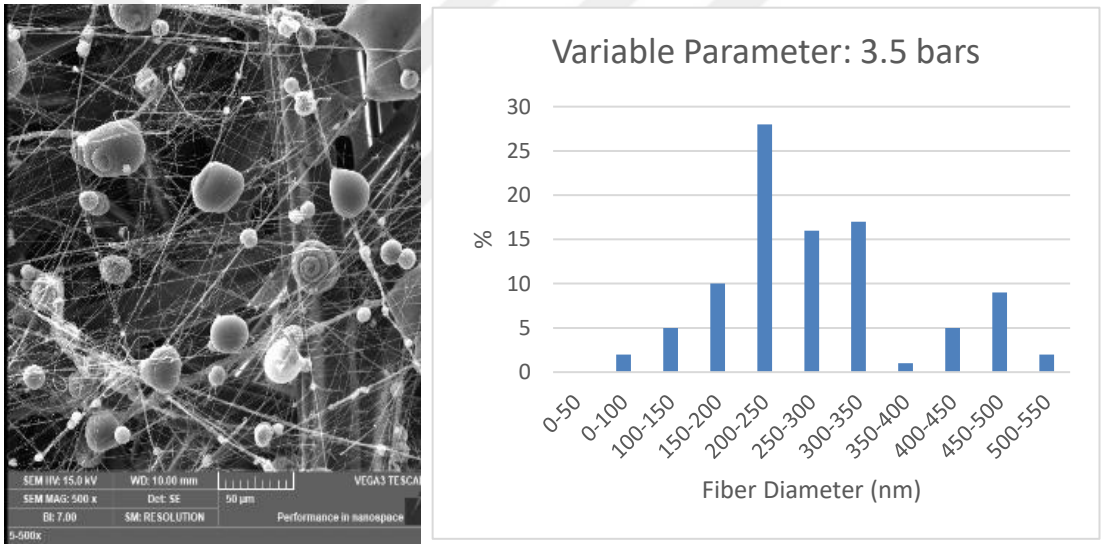

Figure 3.5: (A) SEM image of the sample produced with 5 ml/h, 3.5 bars, %20 PSU/DMF, (B) Nanofiber diameter distribution.

The droplets constitute 65.87% of the total area in the SEM images illustrated in Figure 4.3. SEM image, the droplets compose 13.92% of the completely area (Figure 3.5). SEM image, the droplets constitute 2.49% of the completely area (Figure 3.4).

Figures 3.6, 3.7, and 3.8 shows three distinct productions with 3 bar 20% PSU/DMF content and the effect of feed rate on production, with feed rates of 3 ml/h, 5 ml/h, and 7 ml/h analyzed. Figure 3.6 shows that at a feed rate of 3 ml/h, 36% of the fibre distribution has a diameter around 100 nm . Similarly, Figure 3.7 shows feed rate of 5 ml/h, 26% of the fibre distribution is around 100 nm . Again, as seen in Figure 3.8 feed

rate of 7 ml/h, 28% of the fibre diameter distribution is around 100 nm or less. Comparing the fibre diameter distributions in Figure 3.7 and Figure 3.8, it can be seen that 68% of the fibre diameter distribution in Figure 3.7 is 150 nanometres, while this ratio is 60% in Figure 3.8. Therefore, an overall increase in fibre diameters was observed as the feed rate increased.

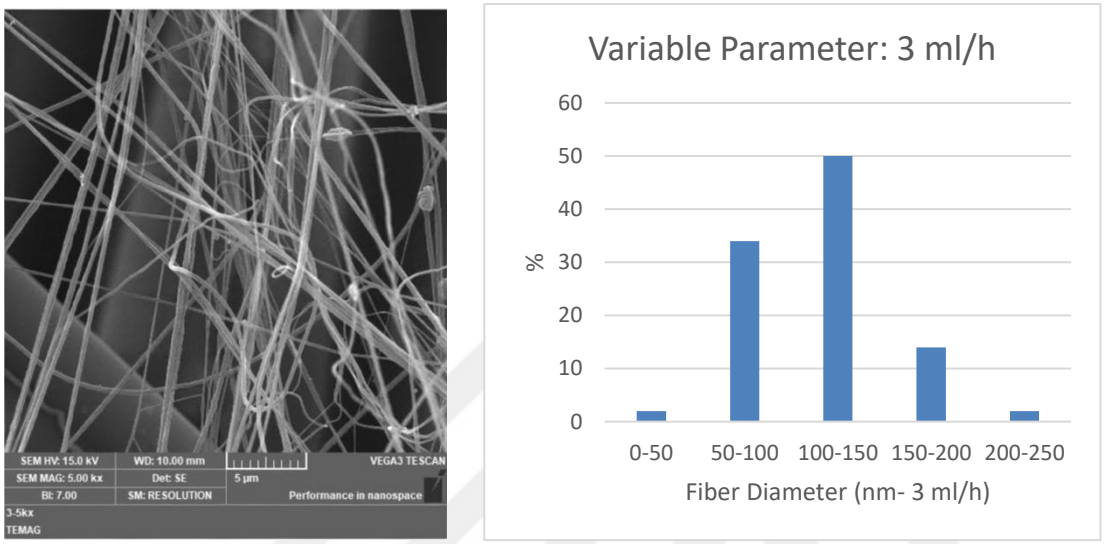

Figure 3.6: (A) SEM image of the sample produced with 3 ml/h, 3 bars, %20 PSU/DMF, (B) Nanofiber diameter distribution.

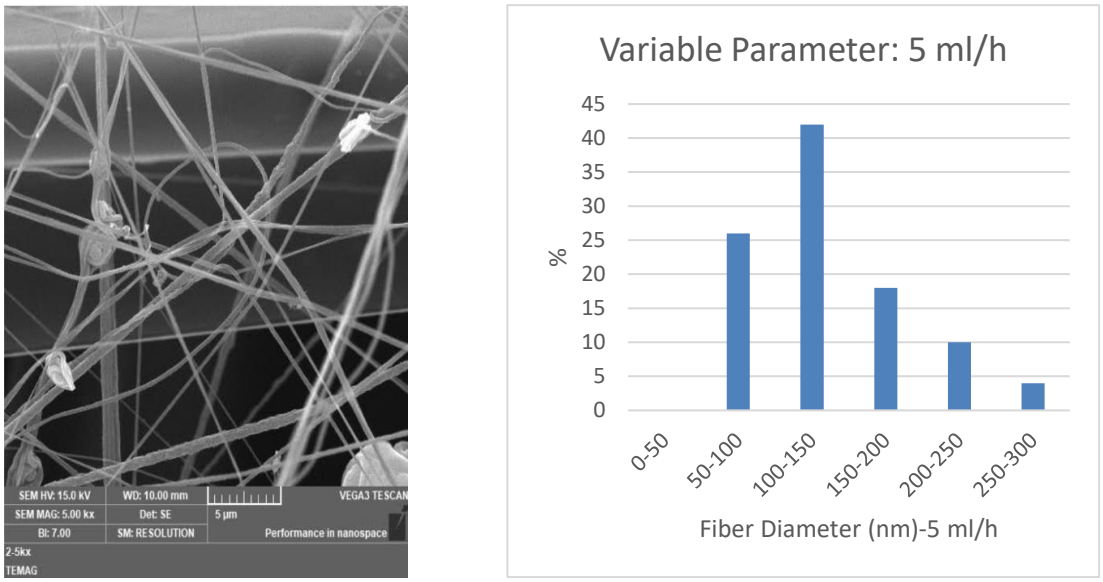

Figure 3.7: (A) SEM image of the sample produced with 5 ml/h, 3 bars, %20 PSU/DMF, (B) Nanofiber diameter distribution.

Figure 3.9, Figure 3.10, and Figure 3.11 were generated using there diffirent feed rates and a 3 bar 20% PSU/DMF solution. To optimize the process, the effect of three different pressure values on droplet diameters was investigated The smallest droplet was observed at a feed rate of 5 ml/h, with droplet diameters measured at feed rates of 3 ml/h, 5 ml/h, 7 ml/h.

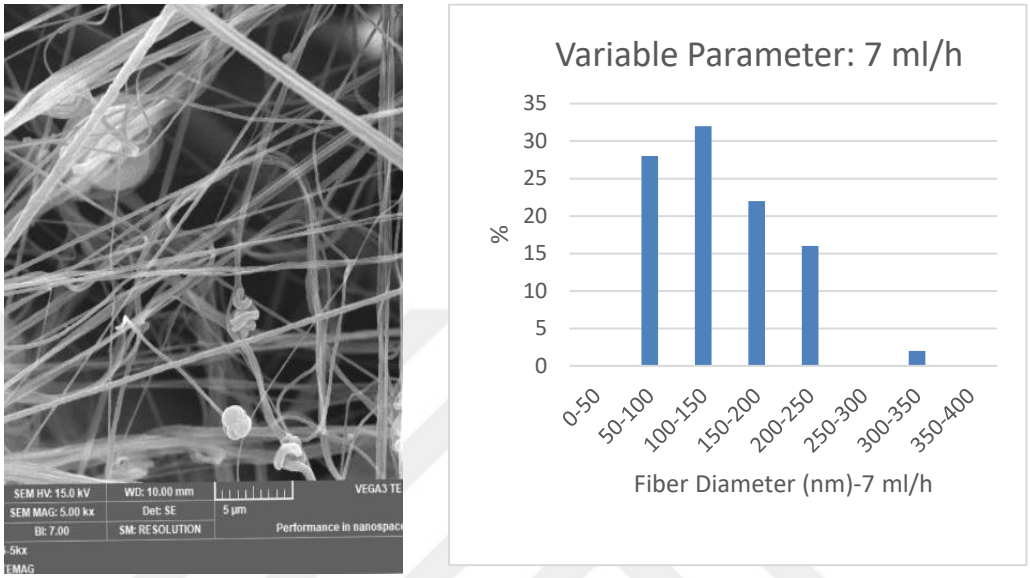

Figure 3.8: (A) SEM image of the sample produced with 7 ml/h, 3 bars, %20 PSU/DMF, (B) Nanofiber diameter distribution.

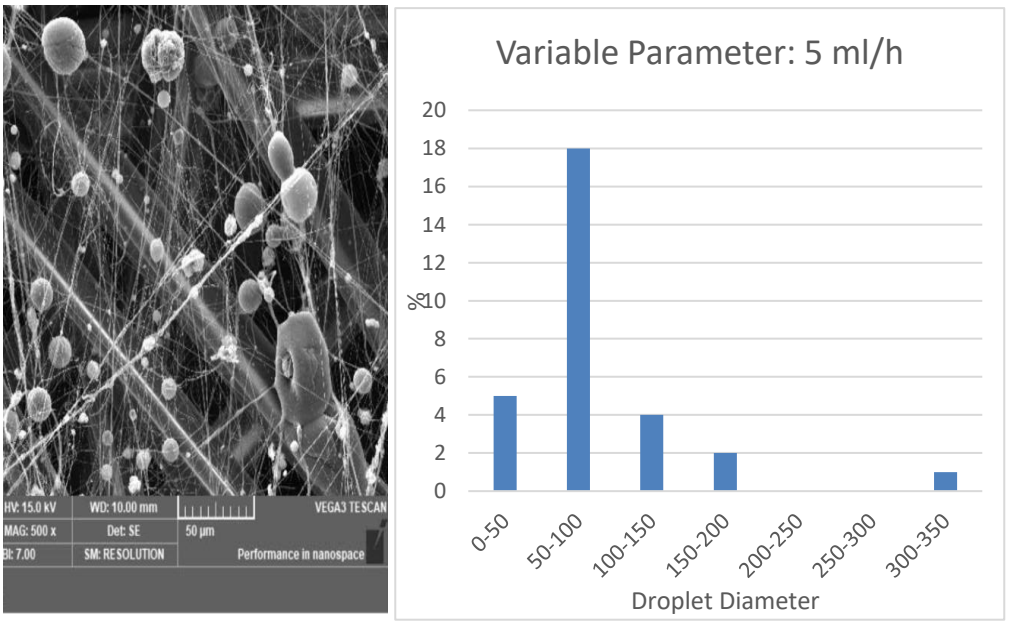

Figure 3.9: (A) SEM image of the sample produced with 5 ml/h, 3 bars, %20 PSU/DMF, (B) Droplet diameter distribution.

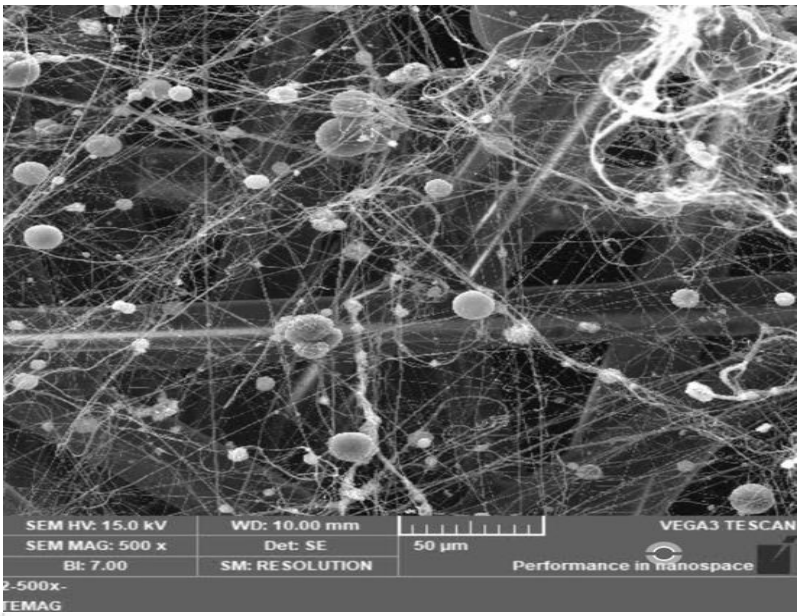

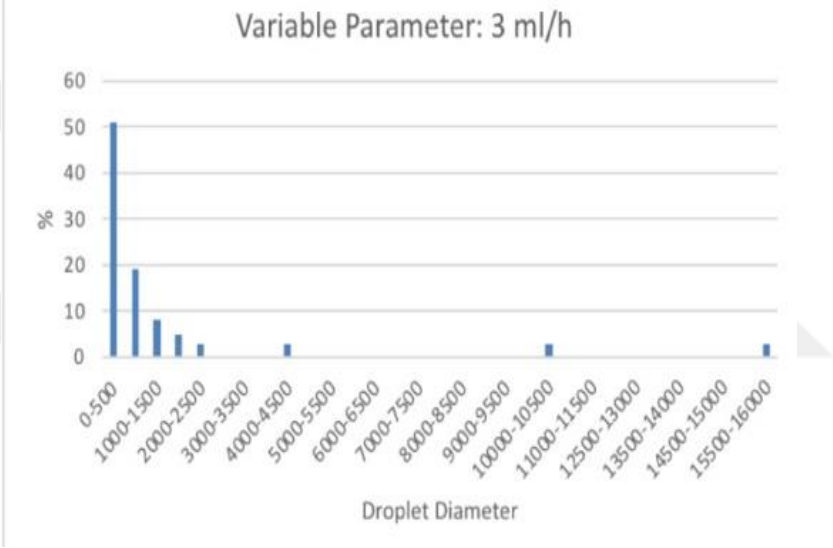

Figure 3.10: (A) SEM image of the sample produced with 3ml/h, 3 bars, %20 PSU/DMF, (B) Droplet diameter distribution.

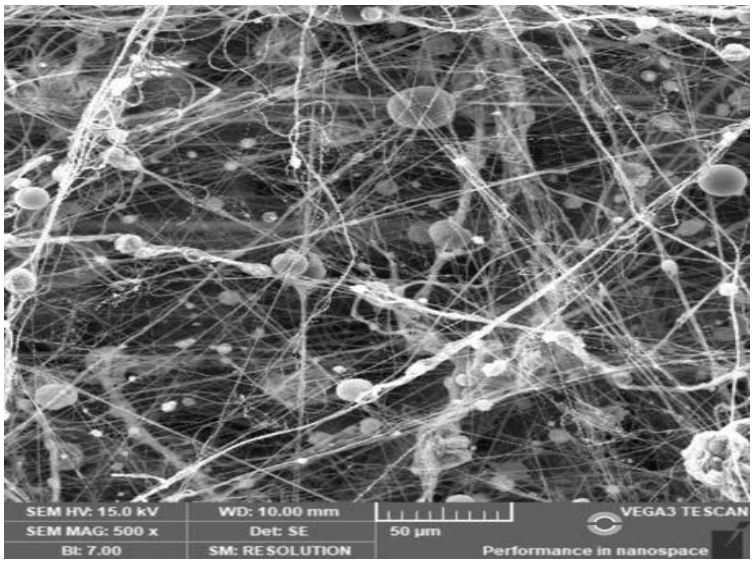

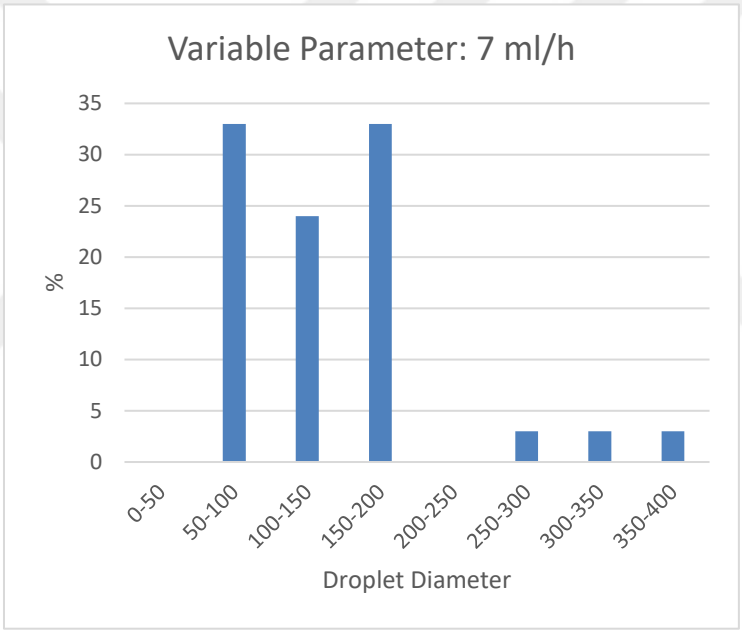

Figure 3.11: (A) SEM image of the sample produced with 7 ml/h, 3 bars, %20 PSU/DMF, (B) Droplet diameter distribution.

Compared to the samples produced for 15 min for optimisation, nanofiber diameters did not exceed 1000 nm at a significant rate in long-term production. However, when the nanofiber diameter distributions were examined, fibre diameters of 1000 nm and above were observed in long-term production(B.1-B.6). When the average void size on the surface of the non-hot pressed samples were examined, it was observed that the average void size of them were above 1000 nm (B.7-B.9).

3.2 The Void Size on The Surface Size Optimization by Hot-press Treatment

The optimization of the hot press was continued until the optimum void size on the surface was achieved, as determined by the results of the polyamide synthesis experiment. Specifically, the determination of the optimum the average void size on the surface was based on the ability of the substrate surface to be coated with polyamide. The void was defined as the voids formed between the nanofibers on the surface. The size of the voids was calculated by taking measurements from several places and averaging them in ImageJ software. Experiments were carried out by changing the time and pressure values for hot press optimisation. SEM images of hot press and distribution graphs of thi void size on the surface samples are given below (Fig. 3.12-Fig. 3.15).

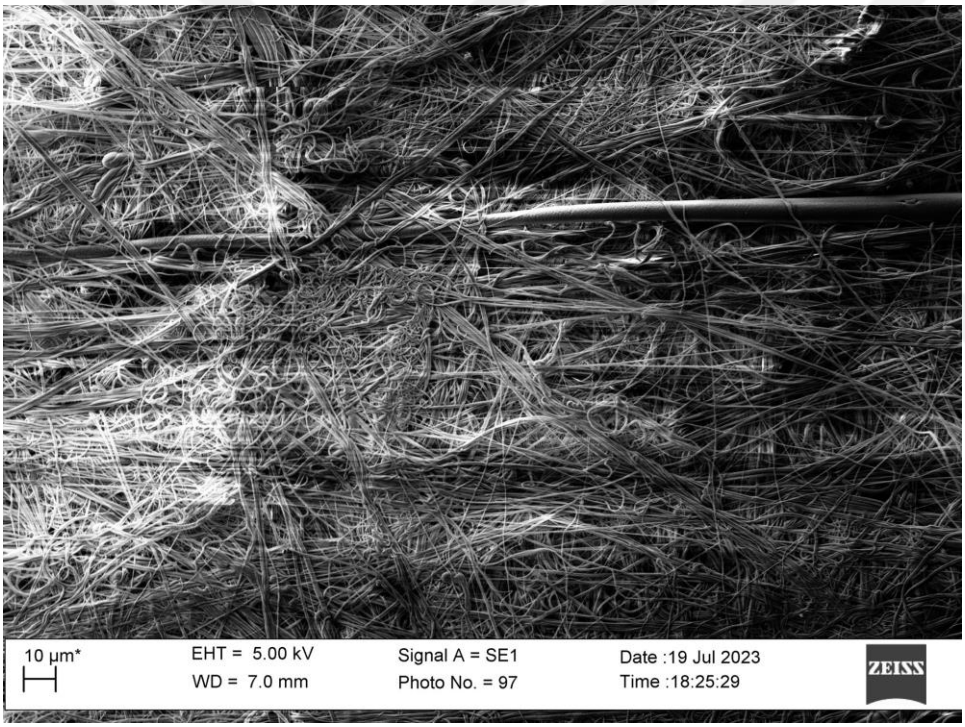

Figure 3.12: SEM images of the sample pressed with 7 bars, 10 minutes-nanofiber produced time is 120 minutes.

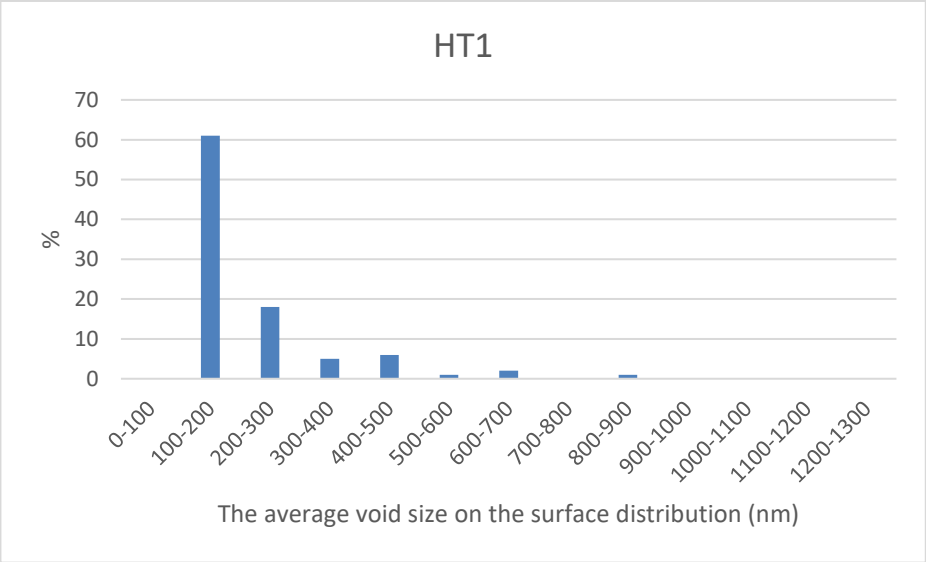

Figure 3.13: The average void size on the surface distribution of the sample 7 bars, 10 minutes, the nanofiber production time is 120 minutes.

The sample with the smallest the average void size on the surface (177.6 nm) of the hot press samples is shown in the Figure 3.18. The substrate with 120 minutes production time was kept at 70^{o} for 10 minutes under 7 bar pressure

The hot press image and void size on the surface distribution shown in the Figure 3.20 belong to the sample produced for 60 minutes. The applied hot press parameters are 5 minutes 5 bar 70 degrees. The average void size on the surface is 526 nm. The effects of hot-press parameters on void size on the surface are analysed in the graph in the Figure 3.16.

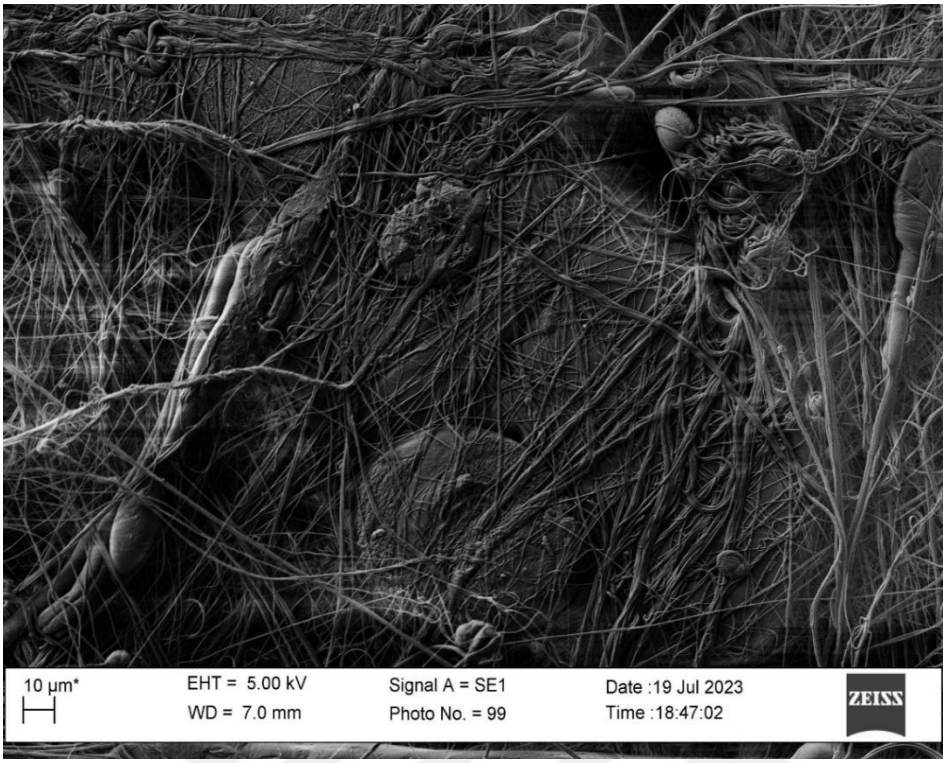

Figure 3.14: SEM images of the sample pressed wih 5 minutes, 5 bars, the production time is 60 minutes.

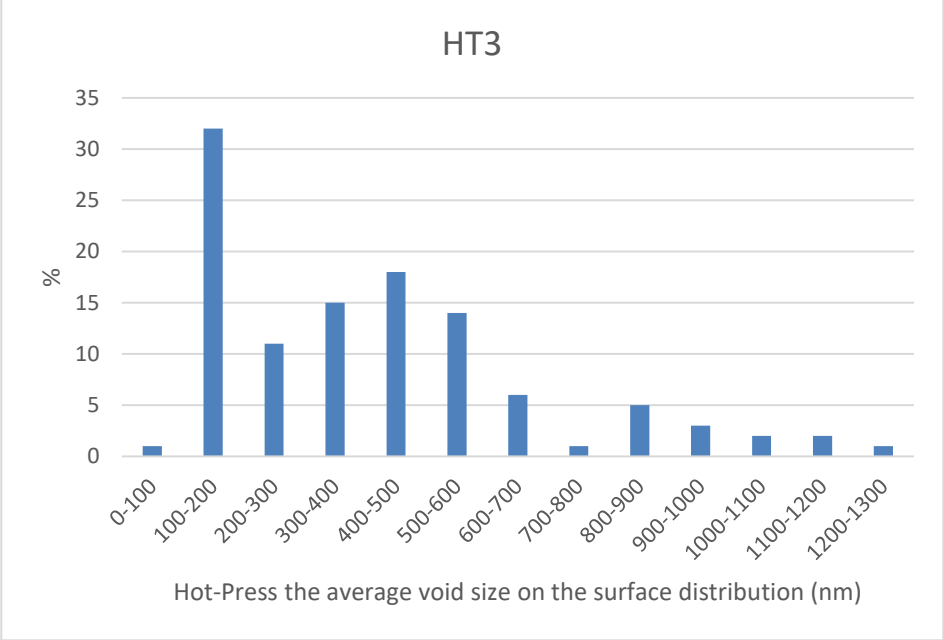

Figure 3.15: The void size of the surface distribution of the sample 5 bars, 5 minutes, the nanofiber production time is 60 minutes.

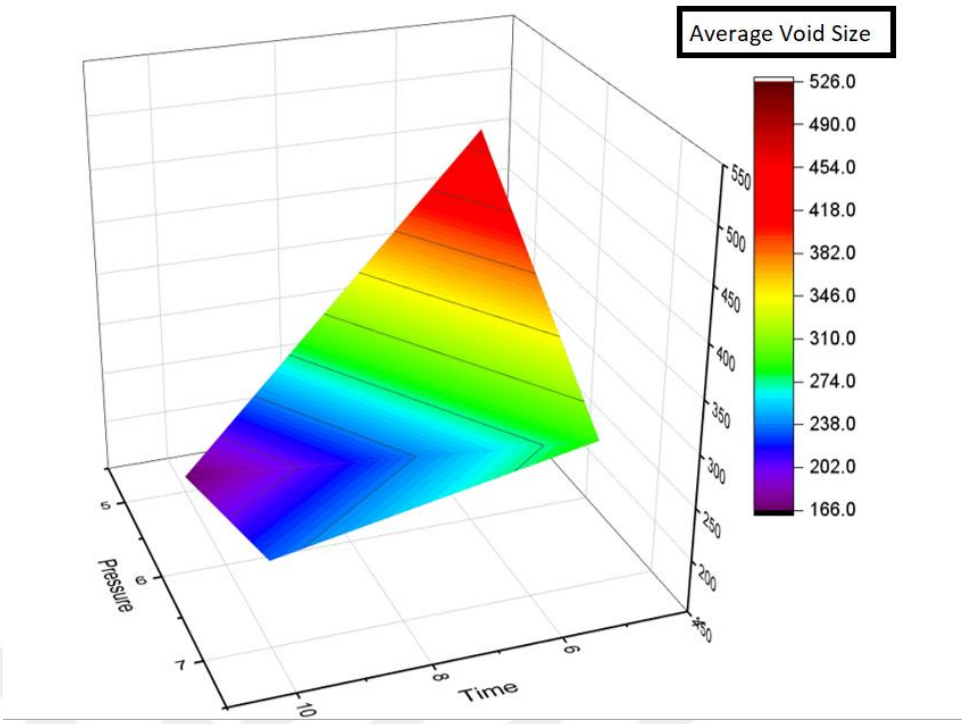

Figure 3.16: Pressure-void size on the surface-time analysis chart.

3.3 Contact Angle Analysis

The hydrophilic properties of the substrate surfaces were analysed by measuring the contact angle. While the non-hot pressed samples had a contact angle between 135^{o} and 134^{o}, it was observed that the hydrophobicity decreased after hot pressing. In 120 minutes of production, contact angle was measured as 124.57^{o} when 7 bar 5 minutes 70^{o} hot press parameters were applied (Figure 3.17). When 120 minutes production 7

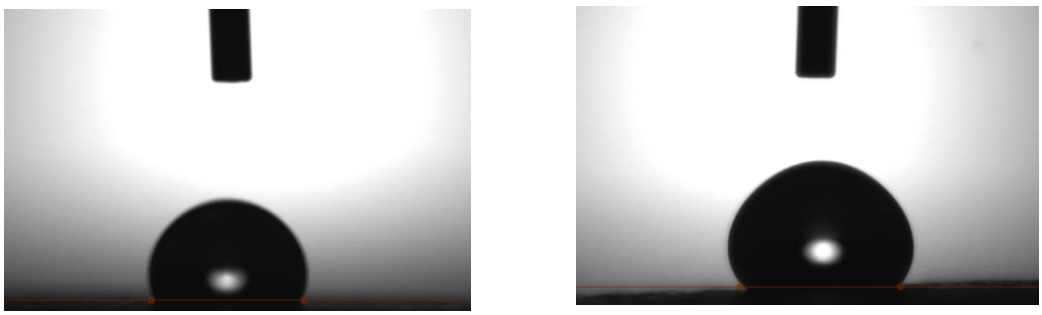

Figure 3.17: (A) Contact angle of the sample pressed with 7 bar 10 minutes (120 minutes is nanofiber production time), (B) Contact angle of the sample pressed with 7 bar 5 minutes (120 minutes is nanofiber production time.

bar 10 minutes hot press parameters were applied, it was observed that the contact angle decreased to 113.07^{o} (Figure 3.18).

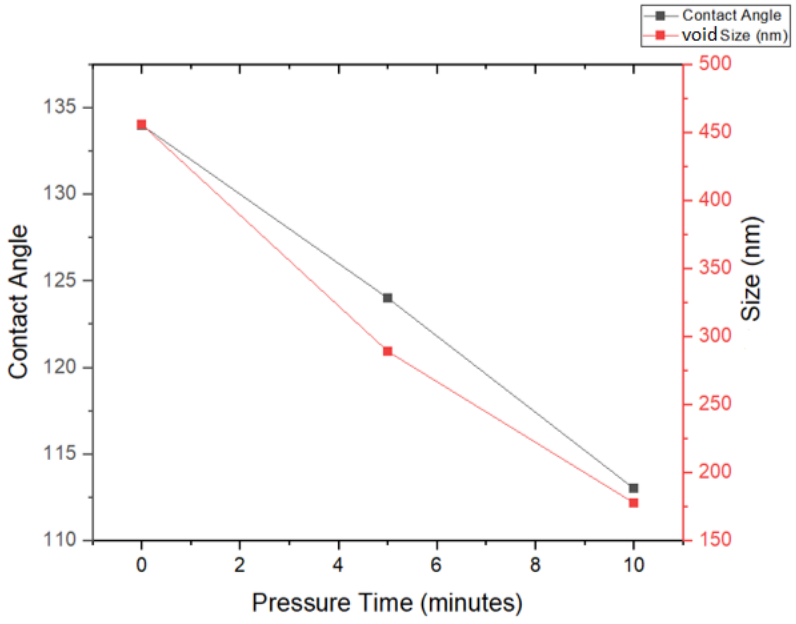

Figure 3.18: Contact angle-void size pressure-time analysis chart.

3.4 Polyamide Synthesis by Interfacial Polymerization Method

Numerous parameters, including the average void size, curing time, monomer concentration, oven temperature, interfacial polymerization techniques, and substrate surface morphology, affect the synthesis of polyamide. The substrate, the duration of contact between the monomers and the substrate surface, and the sequence in which the monomers were added to the reaction were all optimized in this thesis.

3.4.1 Results of polyamide synthesis

SEM and FT-IR devices were used to analyze the polyamide synthesis. SEM was used to examine the yield of void coatings. The FT-IR-IRvice detected the specific peaks of the polyamide thin film and showed whether the synthesis of polyamide was carried out successfully or not.

3.4.1.1 FTIR characterization of polyamide surface

The characteristic peaks of aromatic polyamide produced by interfacial polymerization on polysulfone are C=O, N-H, and C-N [29]. Special peaks for polyamide were demonstrated in the Figure 3.25 1575 cm^{-1}, and 1660 cm^{-1} are represented N-H bending and C-N stretching [30]. 1720 or 1713 cm $^{-1}$ represented C=O band [31]. As Figure 3.25 seen, 1713 $cm^{-1}$and 1667 cm^{-1} are represented characteristic peak for aromatic polyamide, respectively. Furthermore, in the FTIR result in Figure 3.19, 1583 cm^{-1} is assigned to the N-H bending. FTIR results show that the synthesis of polyamide has been successfully carried out.

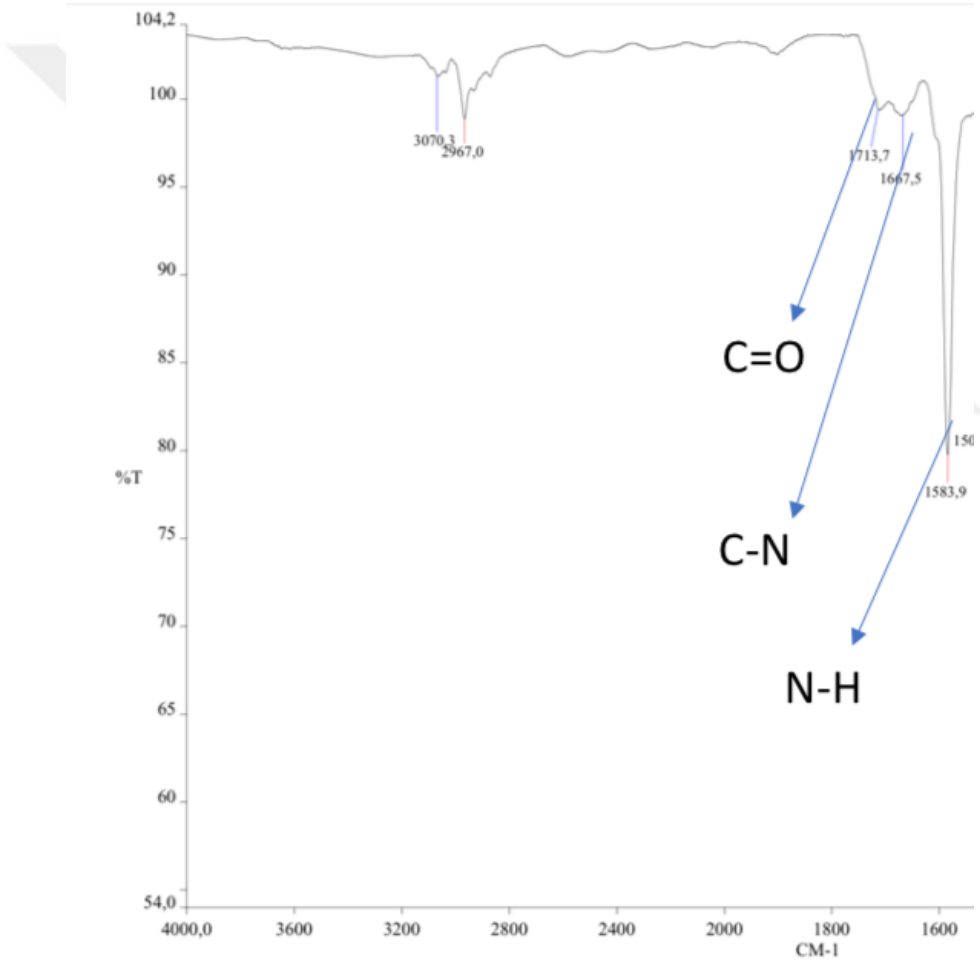

Figure 3.19: FTIR result of polyamide layer.

3.4.1.2 Polyamide synthesis SEM analysis images

First, a non-hot press substrate was used for polyamide synthesis in order to assess the impact of hot press and void size on the process. The sample created using a non-hot press substrate is not suitable for polyamide synthesis, as shown by the SEM pictures

of the sample in Figure 3.20 A. The polyamide synthesis did not have a general surface coverage, despite non-hot-press sample showing a tiny quantity of coating. When applying the hot press treatment, consideration was given to whether the substrate had a polyamide coating. As a result, various substrate samples were subjected to various hot press conditions throughout the polyamide synthesis process.

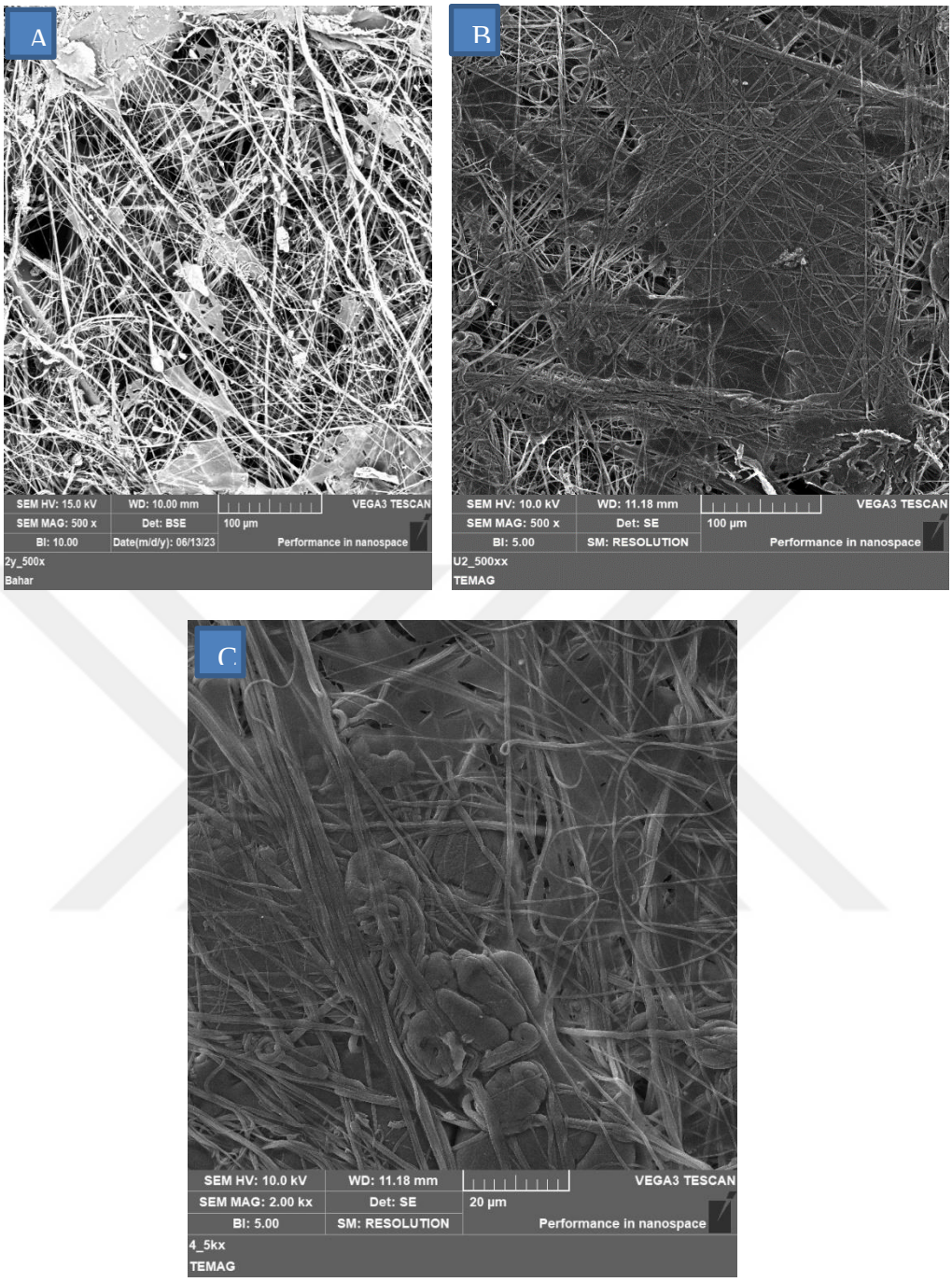

Figure 3.20: Polyamide synthesis on the substrate without hot pressed, (B) the sample was produced for 60 minutes with an application of 5 bar pressure for 10 minutes, (C) the sample was produced for 120 minutes with an application of 5 bar pressure for 10 minutes.

The sample was produced for 60 minutes with an application of 5 bar pressure for 10 minutes at 70 ^{o}C (Figure 3.20 B). Similarly, the sample was produced for 120 minutes with an application of 5 bar pressure for 10 minutes at 70^{o}C (Figure 3.20 C). The surface of the sample in Figure 3.20 C has been coated with polyamide by interfacial polymerization, indicating a high level of quality (Figure 3.20 C).

The substrate surfaces exhibited a super hydrophobic property with an average contact angle of over 130^{o}. The absorption of the MPD aqueous solution was found to be very low due to its hydrophilic structure. In contrast, the TMC-hexane solution was absorbed upon contact with the substrate surface. Because of the hydrophobic surfaces collecting the hydrophilic solution structure in certain areas, MPD solution can't penetrate the pore as shown in the Figure 3.20 A.

When MPD was the first monomer contacted for the synthesis of polyamide, the SEM results shown in the Figure 3.22 and Figure 3.23 were observed. A high degree of coating was visible in the SEM pictures in the Figure 3.23, although 100% coating was not seen. In the FT-IR measurements, particular polyamide peaks were also found, as a result these results show that polyamide synthesis was achived (Figure 3.19). On the other hand, when TMC was the first monomer contacted for the synthesis of polyamide, the SEM result in the Fig. 3.21 was observed. This SEM image demonstrates that, when TMC was the first monomer contact, polyamide synthesis would fail.

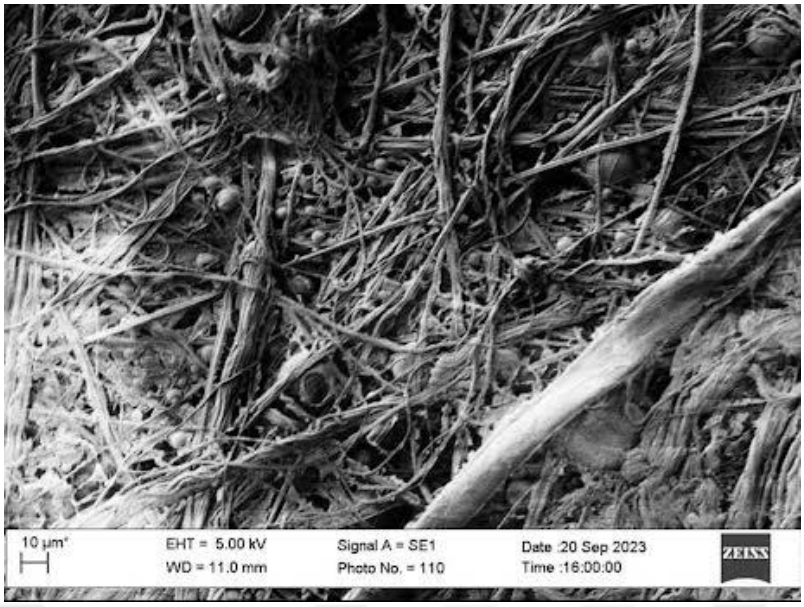

Figure 3.21: The sample formed when the substrate surface was first touched to the TMC organic solution

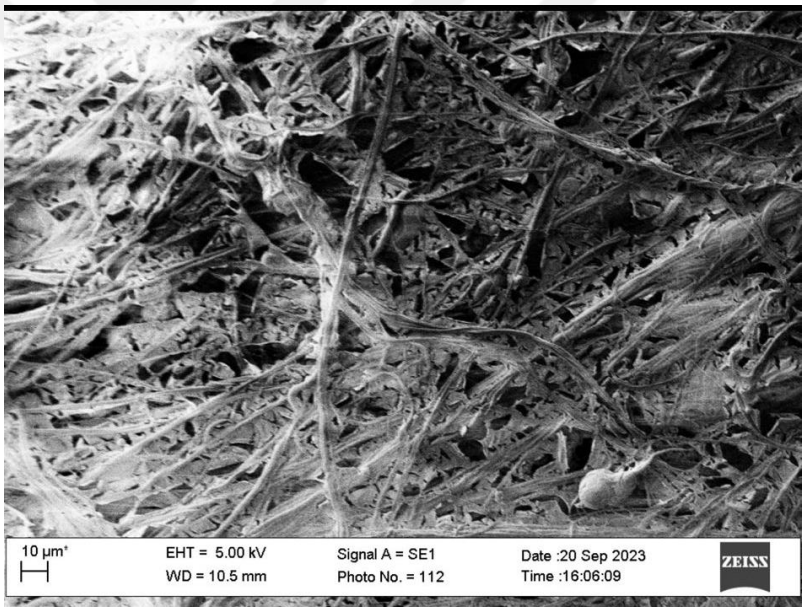

Figure 3.22: Polyamide thin film produced with 20 minutes MPD contact time, 2 minutes TMC contact time.

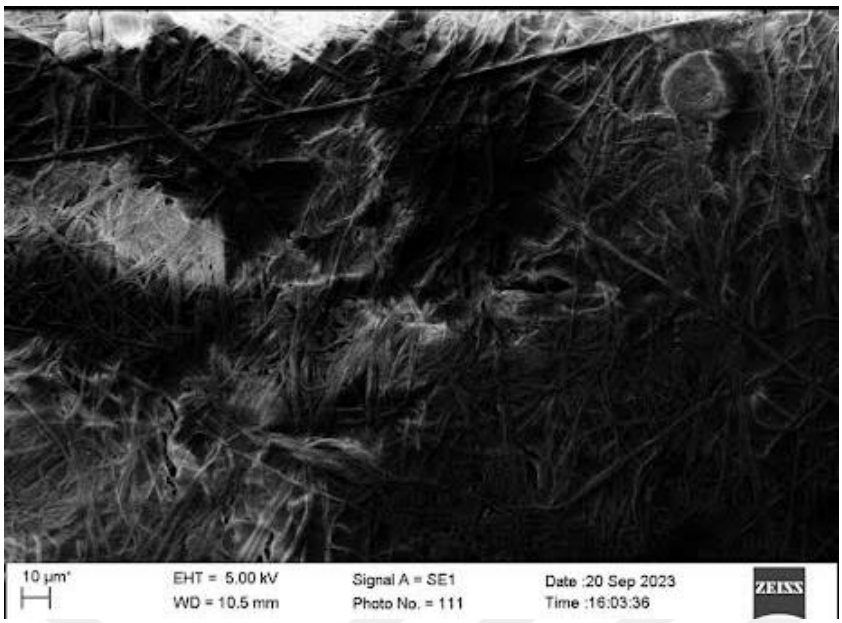

Figure 3.23: Polyamide thin film produced with 20 minutes MPD contact time, 1.5 minutes TMC contact time.

In this study we investigated the impact of contact time between TMC-Hexane monomer solution and MPD aqueous solution on the coating.. Results showed that coating increased with decreasing contact time of TMC-Hexane monomer solution. Additionally, green discoloring was observed on the membranes that were kept after polyamide synthesis on the samples. The experiments revealed that the green discoloring were caused by the interaction of TMC monomers with moisture, as they did not react with MPD. This was confirmed by the appearance of water groups in the FT-IR results. The green discoloring decreased when the TMC-Hexane contact time was reduced (Figure 3.24).

The Figures 3.21 show the SEM images of the experimental results when the TMC-Hexane solution is first contacted with the substrate surface. According to this, no coating was observed on the substrate surface when TMC monomer was the first contacting monomer. The density of TMC-Hexane solution is small compared to the MPD aqueous solution. During polyamide synthesis, MPD molecules diffuse towards the surface of TMC-Hexane solution. As the low-density TMC-Hexane solution is the first monomer to make contact, it settles at the bottom of the solution layers. However, its low density causes it to go up, disrupting the polymerization process and preventing the formation of a thin film [32].

The Figure 3.25 shows a cross-section SEM image of the polyamide membrane sample that was synthesized. During the polyamide synthesis, carbon monoxide gas was released, which caused the thin film to curve and take on a life-like appearance [33]. The image in the Figure displays life-like patterns that formed on the polyamide thin film.

Figure 3.24: Green colour change decreased when TMC-Hexane contact time decreased (to the right).

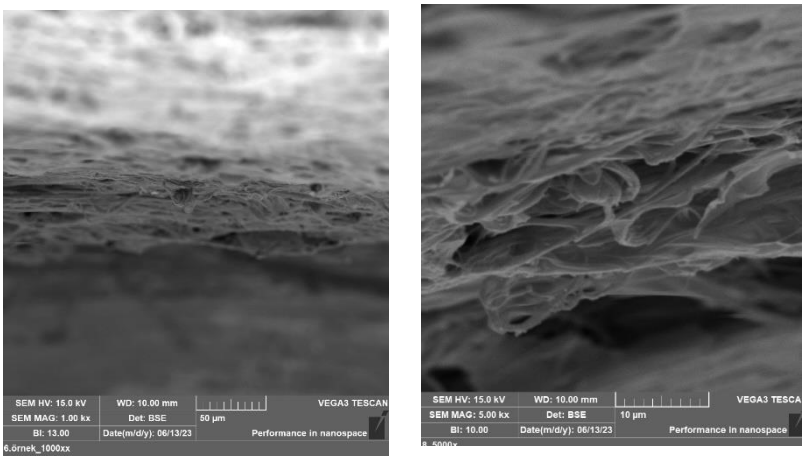

Figure 3.25: (A) SEM image of the polyamide thin film with 1 kx magnification, (B) SEM image of the polyamide thin film with 5 kx magnification.

6. CONCLUSIONS AND RECOMMENDATION

In this thesis, polyamide was synthesised on the optimised nanofiber substrate surface. Furthermore, the nanofiber optimisation process is two-step. Electroblowing and solution-blowing nanofiber production methods were used to optimise the nanofiber. Substrate surfaces produced by electroblowing were hot-pressed to optimise average void size and improve surface properties.

Within the scope of nanofiber optimisation, solution optimisation and system parameter optimisation were performed. For solution optimisation, the polysulfone concentration, NMP, and DMF solvent usage ratios were varied. The optimum solution parameters were determined by droplet size analysis of nanofiber SEM images with ImageJ.

The solution parameters determined in the analyses are as follows: 40 percent NMP, 60 % DMF, and 24 % polysulfone. Electroblowing system parameters are determined as follows: 20 kV voltage, 5 ml/h feed rate, and 3 bar air pressure.

For void size optimisation, first-stage void size optimisation was performed by rotating the substrate surface 90^{o} during the production process and changing the production hours. Surface properties and average void size were optimised by hot pressing. The void size of the surface optimisation analyses were performed using ImageJ software and polyamide synthesis achivement. The optimum hot press parameters and production time determined by these measurements are as follows: 120 minutes of electroblowing production time, 7 bars, 10 minutes, and 70^{o} C. Within the scope of polyamide synthesis, polyamide synthesis was optimised by varying the concentration of the monomer solutions, the contact time of the solutions, and the contact order of the solutions.

No polyamide synthesis was observed when the first contacted monomer solution was contacted with TMC-Hexane solution. MPD and TMC concentrations were determined as 0.5 and 0.005 percent, respectively. Optimum contact times were determined as 3 minutes for MPD aqueous solution and 90 seconds for TMC-Hexane solutio

REFERENCES

[1] **Poh, T. Y., Ali, N. A. T. B. M., Mac Aogáin, M., Kathawala, M. H., Setyawati, M. I., Ng, K. W., & Chotirmall, S. H.** (2018). Inhaled nanomaterials and the respiratory microbiome: clinical, immunological and toxicological perspectives. *Particle and Fibre Toxicology*, *15*, 1-16.

[2] **Saleem, H., Trabzon, L., Kilic, A., & Zaidi, S. J.** (2020). Recent advances in nanofibrous membranes: Production and applications in water treatment and desalination. *Desalination*, *478*, 114-178.

[3] **Bui, N. N., & McCutcheon, J. R.** (2013). Hydrophilic nanofibers as new supports for thin film composite membranes for engineered osmosis. *Environmental Science & Technology*, *47*(3), 1761-1769.

[4] **Sadeghzadeh, A., Bazgir, S., & Shirazi, M. M. A.** (2020). Fabrication and characterization of a novel hydrophobic polystyrene membrane using electroblowing technique for desalination by direct contact membrane distillation. *Separation and Purification Technology*, *239*, 116498.

[5] **Yarin, A. L., Koombhongse, S., & Reneker, D. H.** (2001). Taylor cone and jetting from liquid droplets in electrospinning of nanofibers. *Journal of Applied Physics*, *90*(9), 4836-4846.

[6] **Gao, Y., Zhang, J., Su, Y., Wang, H., Wang, X. X., Huang, L. P., ... & Long, Y. Z.** (2021). Recent progress and challenges in solution blow spinning. *Materials Horizons*, *8*(2), 426-446.

[7] **Al-Qadhi, M., Merah, N., Matin, A., Abu-Dheir, N., Khaled, M., & Youcef-Toumi, K.** (2015). Preparation of superhydrophobic and self-cleaning polysulfone non-wovens by electrospinning: influence of process parameters on morphology and hydrophobicity. *Journal of Polymer Research*, *22*, 1-9.

[8] **Daristotle, J. L., Behrens, A. M., Sandler, A. D., & Kofinas, P.** (2016). A review of the fundamental principles and applications of solution blow spinning. *ACS Applied Materials & Interfaces*, *8*(51), 34951-34963.

[9] **Zhang, L., Kopperstad, P., West, M., Hedin, N., & Fong, H.** (2009). Generation of polymer ultrafine fibers through solution (air-) blowing. *Journal of Applied Polymer Science*, *114*(6), 3479-3486.

[10] **Sarac, Z., Kilic, A., & Tasdelen-Yucedag, C.** (2023). Optimization of electro-blown polysulfone nanofiber mats for air filtration applications. *Polymer Engineering & Science*, *63*(3), 723-737.

[11] **Atif, R., Combrinck, M., Khaliq, J., Hassanin, A. H., Shehata, N., Elnabawy, E., & Shyha**, I. (2020). Solution blow spinning of high-performance submicron polyvinylidene fluoride nanofibers: Computational fluid mechanics modelling and experimental results. *Polymers*, ***12***(5), 1140.

[12] **Atif, R., Combrinck, M., Khaliq, J., Hassanin, A. H., Shehata, N., Elnabawy, E., & Shyha, I.** (2020). Solution blow spinning of high-performance submicron polyvinylidene fluoride nanofibers: Computational fluid mechanics modelling and experimental results. *Polymers*, ***12***(5), 1140.

[13] **Ali TOPTAŞ**, (2019) "Elektro üfleme yöntemiyle üretilen poliamid nanoliflerin

filtrasyon özelliklerinin iyileştirilmesi" (Master Thesis) Department of Textile Engineering Textile Engineering Programme, Istanbul."

[14] **Sarhan, W. A., & Azzazy, H. M.** (2015). High concentration honey chitosan electrospun nanofibers: Biocompatibility and antibacterial effects. *Carbohydrate Polymers*, *122*, 135-143.

[15] **Sarac, Z., Kilic, A., & Tasdelen-Yucedag, C.** (2023). Optimization of electro-blown polysulfone nanofiber mats for air filtration applications. *Polymer Engineering & Science*, *63*(3), 723-737.

[16] **Feng, Y., Han, G., Chung, T. S., Weber, M., Widjojo, N., & Maletzko, C.** (2017). Effects of polyethylene glycol on membrane formation and properties of hydrophilic sulfonated polyphenylenesulfone (sPPSU) membranes. *Journal of Membrane Science*, *531*, 27-35.

[17] **Qiao, S. Z., Yu, C. Z., Hu, Q. H., Jin, Y. G., Zhou, X. F., Zhao, X. S., & Lu, G. Q.** (2006). Control of ordered structure and morphology of large-pore periodic mesoporous organosilicas by inorganic salt. *Microporous and Mesoporous Materials*, *91*(1-3), 59-69.

[18] **Huang, L., & McCutcheon, J. R.** (2015). Impact of support layer void size on performance of thin film composite membranes for forward osmosis. *Journal of Membrane Science*, *483*, 25-33.

[19] **Ghosh, A. K., & Hoek, E. M.** (2009). Impacts of support membrane structure and chemistry on polyamide–polysulfone interfacial composite membranes. *Journal of Membrane Science*, ***336***(1-2), 140-148.

[20] **Kaur, S., Barhate, R., Sundarrajan, S., Matsuura, T., & Ramakrishna, S.** (2011). Hot pressing of electrospun membrane composite and its influence on separation performance on thin film composite nanofiltration membrane. *Desalination*, *279*(1-3), 201-209.

[21] **Yogarathinam, L. T., Gangasalam, A., Ismail, A. F., & Parthasarathy, P.** (2018). Harvesting of microalgae Coelastrella sp. FI69 using pore former induced TiO2 incorporated PES mixed matrix membranes. *Journal of Chemical Technology & Biotechnology*, *93*(3), 645-655.

[22] **Ali, M. E., Wang, L., Wang, X., & Feng, X.** (2016). Thin film composite membranes embedded with graphene oxide for water desalination. *Desalination*, ***386***, 67-76.

[23] **Berezkin, A. V., & Kudryavtsev, Y. V.** (2014). Linear interfacial polymerization: Theory and simulations with dissipative particle dynamics. *The Journal of Chemical Physics*, *141*(19).

[24] **A. Güvensoy**, (2018)"Fabrıcatıon of amino acid functionalized cnt/polyamide thin film nanocomposite desalination membranes Chemical Engineering Programme,"Istanbul.

[25] **Park, S. J., Ahn, W. G., Choi, W., Park, S. H., Lee, J. S., Jung, H. W., & Lee, J. H.** (2017). A facile and scalable fabrication method for thin film composite reverse osmosis membranes: dual-layer slot coating. *Journal of Materials Chemistry A*, *5*(14), 6648-6655.

[26] **Stijnman, A. C., Bodnar, I., & Tromp, R. H.** (2011). Electrospinning of food-grade polysaccharides. *Food Hydrocolloids*, ***25***(5), 1393-1398.

[27] **Qin, Z. Y., Jia, X. W., Liu, Q., Kong, B. H., & Wang, H.** (2019). Fast dissolving oral films for drug delivery prepared from chitosan/pullulan electrospinning nanofibers. *International journal of Biological Macromolecules*, *137*, 224-231.

[28] **Kong, C. S., Yoo, W. S., Lee, K. Y., & Kim, H. S.** (2009). Nanofiber deposition by

electroblowing of PVA (polyvinyl alcohol). *Journal of Materials Science*, *44*, 1107-1112.

[29] **Hermans, S., Bernstein, R., Volodin, A., & Vankelecom, I. F.** (2015). Study of synthesis parameters and active layer morphology of interfacially polymerized polyamide–polysulfone membranes. *Reactive and Functional Polymers*, *86*, 199-208.

[30] **Jin, Y., Wang, W., & Su, Z**. (2011). Spectroscopic study on water diffusion in aromatic polyamide thin film. *Journal of Membrane Science*, *379*(1-2), 121-130.

[31] **Fathizadeh, M., Aroujalian, A., & Raisi, A.** (2012). Effect of lag time in interfacial polymerization on polyamide composite membrane with different hydrophilic sub layers. *Desalination***,** *284*, 32-41.

[32] **Li, J., Wei, M., & Wang, Y.** (2017). Substrate matters: The influences of substrate layers on the performances of thin-film composite reverse osmosis membranes. *Chinese Journal of Chemical Engineering*, ***25***(11), 1676-1684.

[33] **Yan, H., Miao, X., Xu, J., Pan, G., Zhang, Y., Shi, Y., ... & Liu, Y**. (2015). The porous structure of the fully-aromatic polyamide film in reverse osmosis membranes. *Journal of Membrane Science*, *475*, 504-510.

[34] **Lauricella, M., Pisignano, D., & Succi, S.** (2017). Effects of nanoparticles on the dynamic morphology of electrified jets. *Europhysics Letters*, ***119***(4), 44001.

[35] **Polat, Y., Pampal, E. S., Stojanovska, E., Simsek, R., Hassanin, A., Kilic, A., ... & Yilmaz, S.** (2016). Solution blowing of thermoplastic polyurethane nanofibers: A facile method to produce flexible porous materials. *Journal of Applied Polymer Science*, *133*(9).

[36] **Zhang, Y., Benes, N. E., & Lammertink, R. G.** (2015). Visualization and characterization of interfacial polymerization layer formation. *Lab on a Chip*, *15*(2), 575-580.

[37] **Ma, X. H., Yang, Z., Yao, Z. K., Guo, H., Xu, Z. L., & Tang, C. Y.** (2018). Interfacial polymerization with electrosprayed microdroplets: toward controllable and ultrathin polyamide membranes. *Environmental Science & Technology Letters*, *5*(2), 117-122.

APPENDICES

APPENDIX A: Tablo of nanofiber optimization.

APPENDIX B: SEM images and graphs for nanofiber optimization.

APPENDIX A

A.1: Experimental groups of nanofiber opimization.

Experimental Group	Concentration (%)	Solvent	Pressure (Bar)	Feeding Rate (ml/h)
			P2	FR
SA1	%8	DMF	2	5
SA2	%10	DMF	2	5
SA3	%13	DMF	2	5
SA4	%15	DMF	2	5
SA5	%18	DMF	2	5
SA6	%20	DMF	2	5
SA7	%24	DMF	2	5
SB1	%8	DMF	3	5
SB2	%10	DMF	3	5
SB3	%13	DMF	3	5
SB4	%15	DMF	3	5
SB5	%18	DMF	3	5
SB6	%20	DMF	3	5
SB7	%24	DMF	3	5
SF1	%8	DMF	3.5	5
SF2	%10	DMF	3.5	5
SF3	%13	DMF	3.5	5
SF4	%15	DMF	3.5	5
SF5	%18	DMF	3.5	5
SF6	%20	DMF	3.5	5
SF7	%24	DMF	3.5	5
SF8	%25	DMF	3.5	5
SC1	%8	DMF	4	5
SC2	%10	DMF	4	5
SC3	%13	DMF	4	5
SC4	%15	DMF	4	5
SC5	%18	DMF	4	5
SC6	%20	DMF	4	5
SC7	%24	DMF	4	5

Continued A.1

Experimental Group	Concentration (%)	Solvent	Pressure (Bar)	Feeding Rate (ml/h)
			P2	FR
SD1	%8	DMF	2	7
SD2	%10	DMF	2	7
SD3	%13	DMF	2	7
SD4	%15	DMF	2	7
SD5	%18	DMF	2	7
SD6	%20	DMF	2	7
SD7	%24	DMF	2	7
SE1	%8	DMF	3	7
SE2	%10	DMF	3	7
SE3	%13	DMF	3	7
SE4	%15	DMF	3	7
SE5	%18	DMF	3	7
SE6	%20	DMF	3	7
SE7	%24	DMF	3	7
SG1	%8	DMF	3.5	7
SG2	%10	DMF	3.5	7
SG3	%13	DMF	3.5	7
SG4	%15	DMF	3.5	7
SG5	%18	DMF	3.5	7
SG6	%20	DMF	3.5	7
SG7	%24	DMF	3.5	7
SH1	%8	DMF	4	7
SH2	%10	DMF	4	7
SH3	%13	DMF	4	7
SH4	%15	DMF	4	7
SH5	%18	DMF	4	7
SH6	%20	DMF	4	7
SH7	%24	DMF	4	7
SD1	%8	DMF	2	7

Continued

Continued A.1

Experimental Group	Concentration (%)	Solvent	Pressure (Bar)	Feeding Rate (ml/h)
			P2	FR
SI1	%20	DMF	3	3
SI2	%8	DMF	2	3
SI3	%10	DMF	2	3
SI4	%13	DMF	2	3
SI5	%15	DMF	2	3
SI6	%18	DMF	2	3
SI7	%20	DMF	2	3
SI8	%24	DMF	2	3
SF1	8	DMF	3	3
SF2	10	DMF	3	3
SF3	13	DMF	3	3
SF4	15	DMF	3	3
SF5	18	DMF	3	3
SF6	20	DMF	3	3
SF7	24	DMF	3	3
ST1	8	DMF	3.5	3
ST2	10	DMF	3.5	3
ST3	13	DMF	3.5	3
ST4	15	DMF	3.5	3
ST5	18	DMF	3.5	3
ST6	20	DMF	3.5	3
ST7	24	DMF	3.5	3
SL1	8	DMF	4	3
SL2	10	DMF	4	3
SL3	13	DMF	4	3
SL4	15	DMF	4	3
SL5	18	DMF	4	3
SL6	20	DMF	4	3
SL7	24	DMF	4	3

APPENDIX B

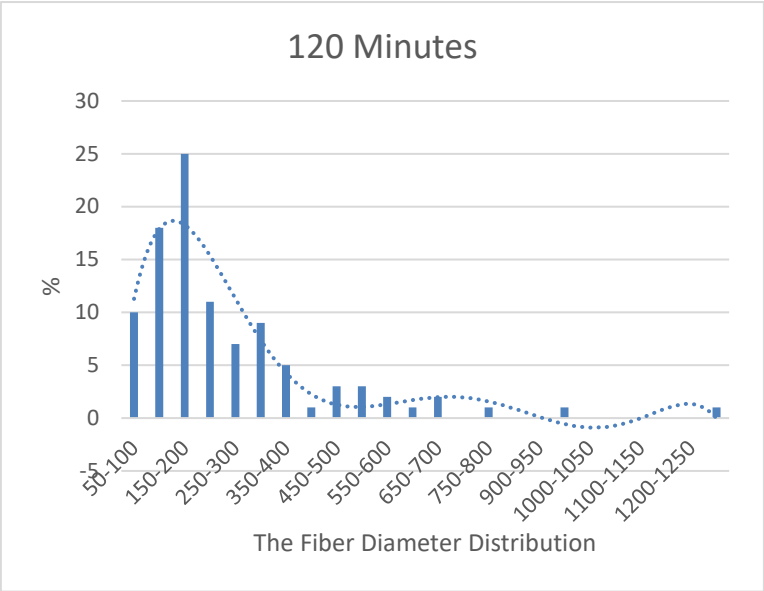

B.1: Nanofiber distribution of the sample PSU produced for 120 minutes.

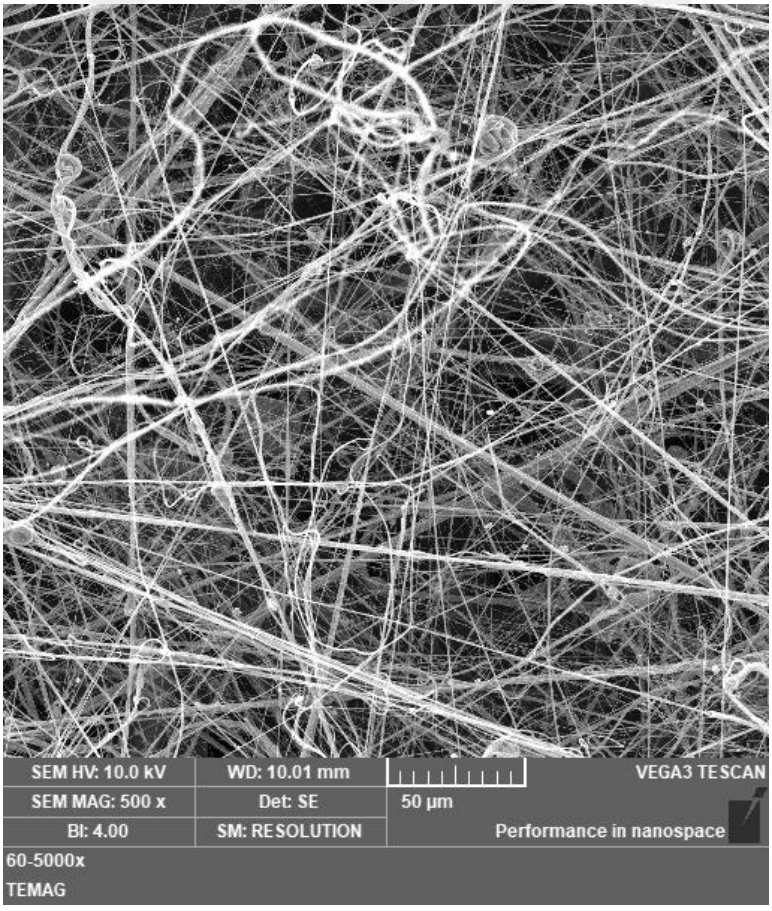

B.2: SEM image of the sample produced 120 minutes.

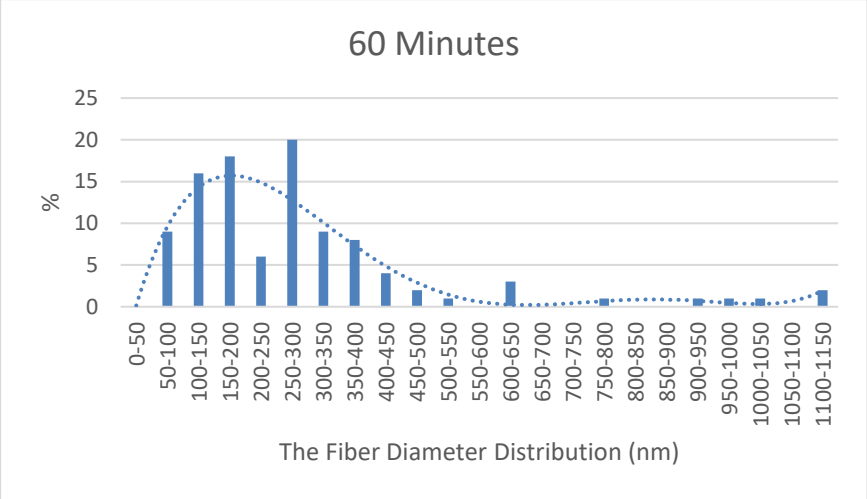

B.3: Nanofiber distribution of the sample PSU produced for 60 minutes.

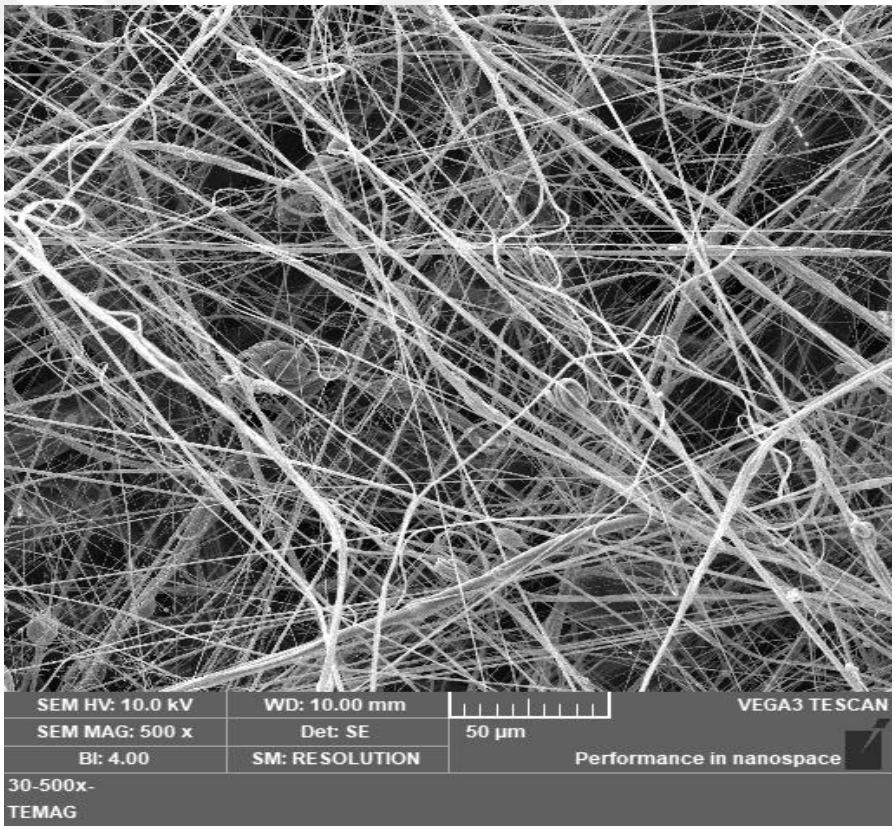

B.4: SEM image of the sample produced with 5 ml/h, 3 bars, %25 PSU/DMF, 20 kV, 60 minutes.

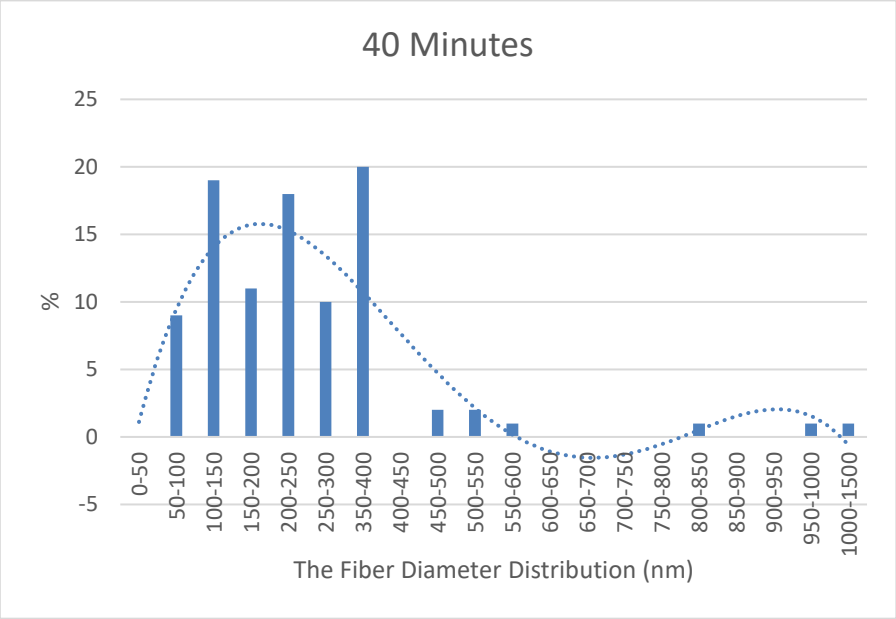

B.5: Nanofiber distribution of the sample PSU produced for 40 minutes.

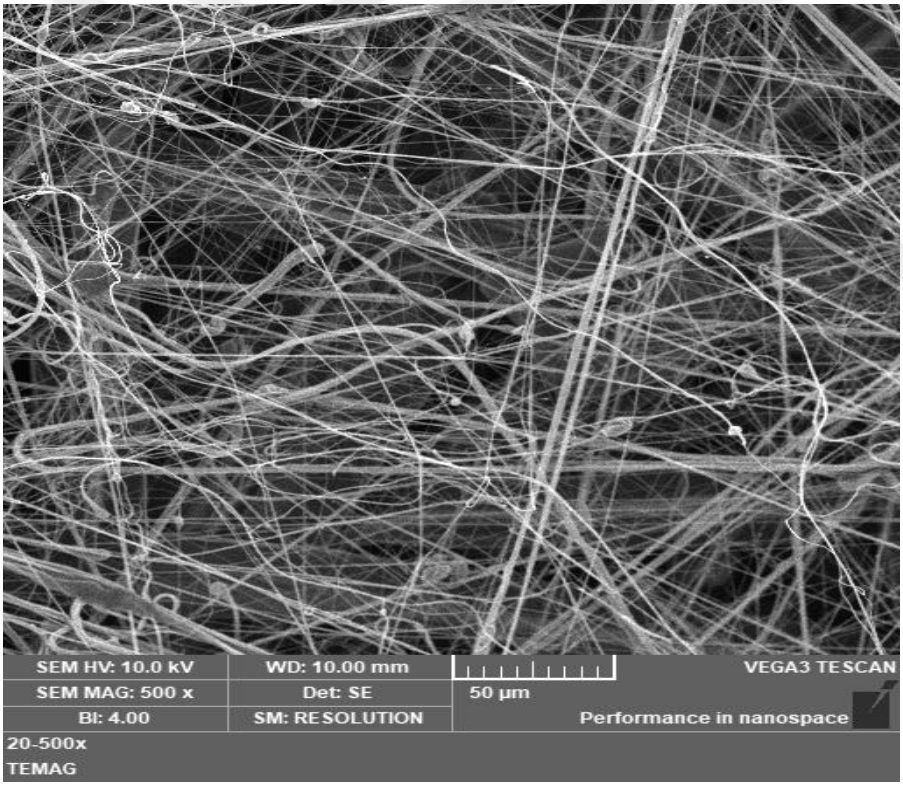

B.6: SEM image of the sample produced with 5 ml/h, 3 bars, %25 PSU/DMF, 20 kV, for 40 minutes.

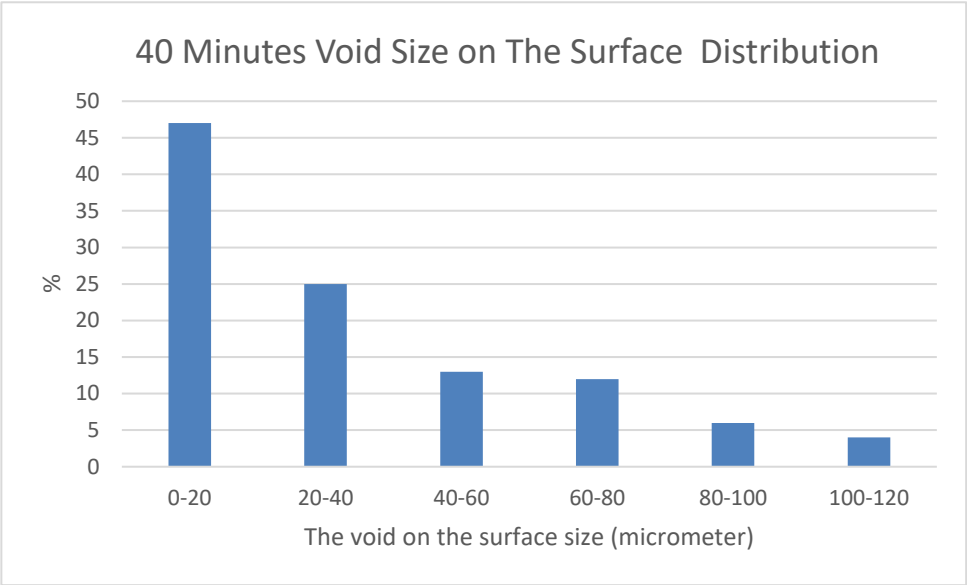

B.7: The void on the surface size distribution for the sample produced for 40 minutes.

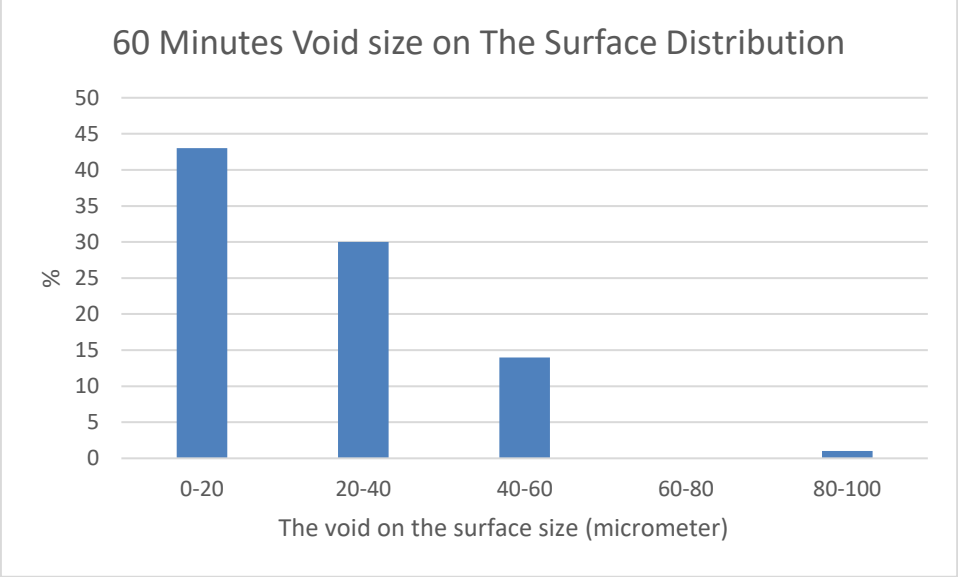

B.8: The void on the surface size distribution for the sample produced for 60 minutes.

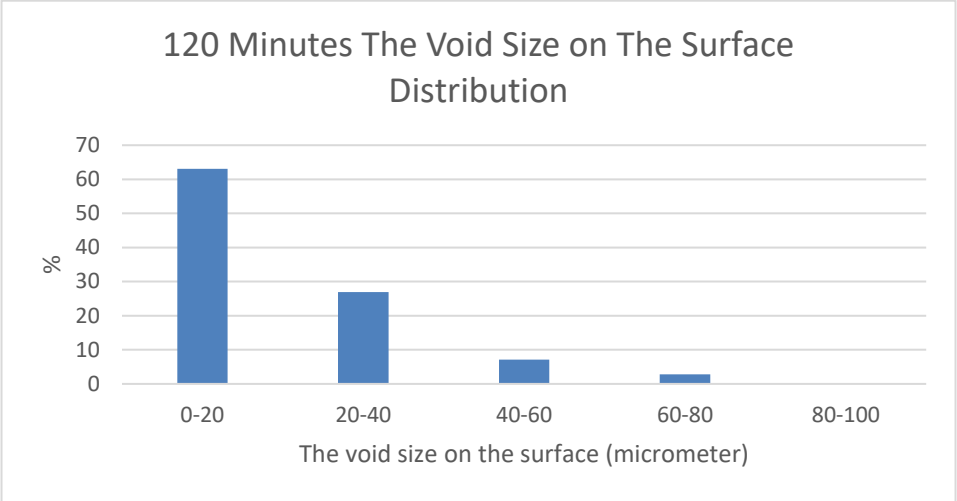

B.9: The void size on the surface for the sample produced for 120 minutes.

CURRICULUM VITAEL

Name Surname: Büşra ARSLAN

EDUCATION

B.Sc: Beykent University, Mechanical Engineering, 2018.
M.Sc: Istanbul Technical University, Nanoscience and Nanoengineering, 2024.

PUBLICATIONS, PRESENTATIONS AND PATENTS ON THE THESIS:

Büşra ARSLAN, Levent TRABZON, (2022). Graphene Oxide Synthesise for Polyamide Thin Film Composite Reverse Osmosis Membrane. International Graduate Research Symposium : IGRS'22, *(1)*, 274.

OTHER PUBLICATIONS, PRESENTATIONS AND PATENTS:

Esra Şerife PAMPAL, Büşra ARSLAN, Ali DEMİR, (2023). Recovery of carbon fiber from prepreg using physical and chemical treatment. International Fiber and Polymer Research Symposium, *(13),* 215-218.